Summer 7-25-2021

Single-crystal elasticity of tremolite at high-pressure conditions and its implication for the mid-lithospheric discontinuity

Soisiri Charin
University of New Mexico

Soisiri Charin
Candidate

Earth and Planetary Sciences
Department

This thesis is approved, and it is acceptable in quality and form for publication:

Approved by the Thesis Committee:

Asst. Prof. Jin Zhang , Chairperson

Prof. Adrian Brearley

Assoc. Prof. Brandon Schmandt

SINGLE-CRYSTAL ELASTICITY OF TREMOLITE AT HIGH-PRESSURE CONDITIONS AND ITS IMPLICATION FOR THE LITHOSPHERIC-DISCONTINUITY

BY

SOISIRI CHARIN

BACHELOR OF ARTS, UNIVERSITY OF COLORADO

THESIS

Submitted in Partial Fulfillment of the

Requirements for the Degree of

Master of Science
Earth and Planetary Sciences

The University of New Mexico

Albuquerque, New Mexico

December 2021

ACKOWLEDGMENTS

I would like to thank my supervisor, Dr. Jin Zhang, for her guidance throughout my graduate career and continuous supports in numerous aspects during my time at UNM. I'm deeply thankful for her commentary and suggestions for my presentation and the dissertation manuscripts. I'm truly grateful for the opportunities that I have been offered here. Her insights, positivity, and encouragement have inspired and bolstered me throughout this project.

I am also grateful for all the inputs from Dr. Adrain Brearley, especially his exceptional understanding of mineralogy and crystallography that have helped me grasp the complexity of the amphiboles. I would like to thank Dr. Brandon Schmandt for his advice on the seismicity and geophysics implication for this project and Dr. Gary Weissmann for his supports and encouragement during my proposal processes.

I am truly thankful to all the staffs in the Department of Earth and Planetary Sciences for the numerous assistances, kindness, and optimism that have given me such strengths and comforts. I'm grateful to all my colleagues in the High-pressure mineral physics lab including Ming Hao, Wenyi Zhou, Rose Hurlow, Wade Mans, and Minguiang Hou for their supports, useful discussion, and laboratory guidance.

I would like to thank Dr. Ying-Bing Jiang for his facilitation for my crystal measurements and Dr. Przemyslaw Dera and the Hawaii Institute of Geophysics and Planetary for the x-ray diffraction analysis of my crystals. I am also thankful for all the supports and accommodation from the OEADC and the Royal Thai Embassy throughout my academic journey in the US.

Lastly, I wish to express my gratitude to my family and friends for their hopeful advice and constant supports (PS, PC, SD, ST, PC, PL, FSTF, KP, EP, and MS).

Single-crystal elasticity of tremolite at high-pressure conditions and its implication for the mid-lithospheric discontinuity

By

Soisiri Charin
B.A., Geological Sciences, University of Colorado Boulder, 2019
M.S., Earth and Planetary Sciences, 2021

ABSTRACT

Tremolite is the calcium magnesium amphibole that widely occurs in igneous and metamorphic rocks of the crustal and upper mantle lithosphere, especially in the greenschist facies to amphibolite facies of ultramafic assemblages. The stability field of amphibole reaches 3-4 GPa and 1100-1200°C depending on water content and cation substitutions giving rise to amphibole to occur in highly variable compositions. This P-T condition, corresponding to the depth about 80-120 km, coincides with the depth range that a negative velocity gradient usually found within most stable cratonic lithospheres. This depth range is seismically called Mid-lithosphere discontinuity (MLD). The geologic processes that might generate the MLD include partial melting, elastically accommodated grain boundary sliding, radial and azimuthal anisotropy, and layering of hydrous minerals by metasomatism or subsequent accretion. In this study, we focus on the hypothesis of layered metasomatized hydrous minerals, in particular, tremolite. The elasticity and anisotropy parameters of single-crystal tremolite from 0 to 7 GPa are obtained through the Brillouin experiments, x-ray diffraction, and the Thermal EOS fit: Ks_0= 86±6 GPa, G_0= 59±4 GPa , Ks'=7.5±1.1, G'=1.9±1. The results from Voigt-Ruess-Hill averaging scheme indicted that the K^{VRH} and G^{VRH} increases with pressure, similar to

previous studies. Our Ks_0, G_0, Ks', and G' are in reasonable agreement with previous studies. The anisotropy indices of tremolite in this study suggested that tremolite is more anisotropic than other major upper mantle minerals throughout the investigated pressure range. The limited data of tremolite here seems in support of the possible contribution of amphiboles to the seismic observations near MLD. However, the data presented in this study only include the velocity measurements from one crystallographic direction due to the spectral quality. Further investigations of amphibole at simultaneously high pressure-temperature conditions along different crystallographic directions are needed to evaluate its role in generating the MLD under cratons.

TABLE OF CONTENTS

LIST OF FIGURES ..... **IX**

LIST OF TABLES ..... **XI**

1. BACKGROUND **1**

1.1 CRYSTAL STRUCTURE AND CHEMISTRY OF TREMOLITE 1

1.2 MID-LITHOSPHERIC DISCONTINUITY 4

1.3 HYDROUS MINERALS AND METASOMATISM 7

1.4 SINGLE-CRYSTAL ELASTICITY 9

1.5 ANISOTROPY 10

2. METHOD **12**

2.1 DIAMOND ANVIL CELL (DAC) 12

2.2 SAMPLE PREPARATION 13

2.3 ELECTRON PROBE MICROANALYSIS (EPMA) 13

2.4 X-RAY DIFFRACTION (XRD) 13

2.5 SINGLE-CRYSTAL BRILLOUIN SPECTROSCOPY 14

2.6 DERIVATION OF THE SINGLE-CRYSTAL ELASTIC PROPERTIES 15

3. RESULTS AND DISCUSSION **18**

3.1 EQUATION OF STATE OF TREMOLITE 18

a. Unit cell parameters at ambient condition 18

b. High-pressure normalized V/V_0 19

3.2 ELASTIC PROPERTIES OF TREMOLITE AT AMBIENT CONDITION 21

a. Comparison of Ks and G with previous studies 21

b. Comparison of Cijs with previous studies 21

c. Comparison of ambient velocity with other upper mantle minerals 25

3.3 ELASTIC PROPERTIES OF TREMOLITE AT HIGH-PRESSURE CONDITIONS 27

a. Aggregate elastic properties at high-pressure condition (Ks, G, Vp, and Vs) 27

b. C_{ij}s at high-pressure conditions 28

c. Anisotropy indices of tremolite and other mantle minerals 32

4. IMPLICATIONS 36

4.1 PETROLOGICAL AND GEOCHEMICAL EVIDENCE OF THE MLD 36

4.2 PROPOSALS OF THE ABUNDANCE OF AMPHIBOLE AT THE MLD DEPTH 37

4.3 VELOCITY COMPARISON AND ANISOTROPY 38

5. CONCLUSION 40

APPENDIX 42

REFERENCE 46

LIST OF FIGURES

FIGURE1 .1.1 STRUCTURAL MODEL OF TREMOLITE (KONG ET AL. 2018) 1

FIGURE 1.2.1 CHANGE IN AZIMUTHAL ANISOTROPY UNDERNEATH NORTH AMERICAN CRATON (YUAN AND ROMANOWICZ 2010) 4

FIGURE 1.2.2 THE EXPERIMENTAL SOLIDUS (SELWAY ET AL. 2015) 6

FIGURE 1.3.1 (A) EXPERIMENTS ON AMPHIBOLE STABILITY 9

FIGURE 1.3.1 (B) MODAL COMPOSITIONS OF THE LITHOSPHERIC MANTLE CORRESPONDING TO SHEAR WAVE VELOCITY REDUCTION 9

FIGURE 2.1.1 THE TREMOLITE SAMPLE LOADED IN DAC SAMPLE CHAMBER..... 12

FIGURE 2.5.1 A TYPICAL BRILLOUIN SPECTRUM OF SINGLE-CRYSTAL TREMOLITE AT 300K AND 7.7 GPA 15

FIGURE 3.1.1 NORMALIZED VOLUME (V/V_0) OF SINGLE-CRYSTAL TREMOLITE..... 20

FIGURE 3.2.1 THE 13 INDEPENDENT ELASTIC MODULI OF TREMOLITE AMPHIBOLE AT AMBIENT CONDITION. 22

FIGURE 3.2.2 MEASURED VELOCITIES OF SINGLE CRYSTAL TREMOLITE AT AMBIENT CONDITION AS A FUNCTION OF CHI ANGLE..... 23

FIGURE 3.2.3 VP OF TYPICAL MINERALS COMPARED WITH TREMOLITE IN THIS STUDY ... 26

FIGURE 3.2.4 VS OF TYPICAL MINERALS COMPARED WITH TREMOLITE IN THIS STUDY.... 26

FIGURE 3.3.1 THE VP, VS, KS, AND G OF SINGLE-CRYSTAL TREMOLITE AT HIGH-P AND ROOM-T CONDITIONS..... 28

FIGURE 3.3.2 MEASURED VELOCITIES OF TREMOLITE AS A FUNCTION OF THE CHI ANGLES AT 1.6 GPA. 29

FIGURE 3.3.3 SINGLE-CRYSTAL ELASTIC MODULI OF TREMOLITE AT DIFFERENT PRESSURES IN THIS STUDY AND PENG AND MOKHERJEE (2020) 31

FIGURE 3.3.4 THE ANISOTROPY UNIVERSAL INDEX (A^U) OF SINGLE-CRYSTAL TREMOLITE AT 300K 32

FIGURE 3.3.5 A^{Vp} OF SINGLE-CRYSTAL TREMOLITE AT 300K FROM SINGLE-CRYSTAL TREMOLITE AT 300K..... 33

FIGURE 3.3.6 A^{Vs} OF SINGLE-CRYSTAL TREMOLITE AT 300K FROM SINGLE-CRYSTAL TREMOLITE AT 300K..... 34

FIGURE 3.3.7 D^{Vs} OF SINGLE-CRYSTAL TREMOLITE AT 300K FROM SINGLE-CRYSTAL TREMOLITE AT 300K..... 35

FIGURE 4.1.1 METASOMATIZED AMPHIBOLE-BEARING ECLOGITE FOUND UNDER CENTRAL KAAPVAAL CRATON (SMART ET AL. 2021) 36

FIGURE S1A PHOTOGRAPHS OF THE SAMPLE CHAMBERS INSIDE THE DAC ASSEMBLY OF SINGLE-CRYSTAL TREMOLITE 42

FIGURE S1B TWO TREMOLITE CRYSTALS WERE PLACED IN THE DAC FOR THE X-RAY DIFFRACTION EXPERIMENTS..... 42

FIGURE S2A A HAND SPECIMEN OF TRE1 SAMPLE 42

FIGURE S2B A POLISHED SINGLE-CRYSTAL TREMOLITE UNDER MICROSCOPE 42

FIGURE S3: BRILLOUIN SPECTRA OF TRE1 UNDER DIFFERENT PRESSURE CONDITIONS... 44

FIGURE S4: ACOUSTIC VELOCITY MEASUREMENTS OF THE 4:1 METHANOL-ETHANOL MIXTURE AS A PRESSURE MEDIUM IN THE BRILLOUIN EXPERIMENTS..... 45

LIST OF TABLES

TABLE 2.1 CHEMICAL COMPOSITION OF TREMOLITE FROM THE EPMA ANALYSIS 14

TABLE 3.1 COMPARISON OF NORMALIZED VOLUME (V/V_0) AT 300 K OF THIS STUDY WITH PREVIOUS PUBLICATION 19

TABLE 3.2. SUMMARY OF TREMOLITE'S ELASTIC PROPERTIES FROM THIS STUDY AND PREVIOUS PUBLICATION 24

TABLE 3.3 VELOCITY OF MANTLE MINERALS AT 300 K AND 0 GPA..... 25

TABLE 3.4 SINGLE-CRYSTAL AND AGGREGATE ELASTIC PROPERTIES OF OMPHACITE AT DIFFERENT PRESSURES DETERMINED IN THIS STUDY 30

TABLE S1. CHEMICAL ANALYSIS OF TREMOLITE AMPHIBOLES FOR THIS PROJECT AND PREVIOUS ELASTICITY STUDY 43

1. Background

1.1 Crystal structure and chemistry of tremolite

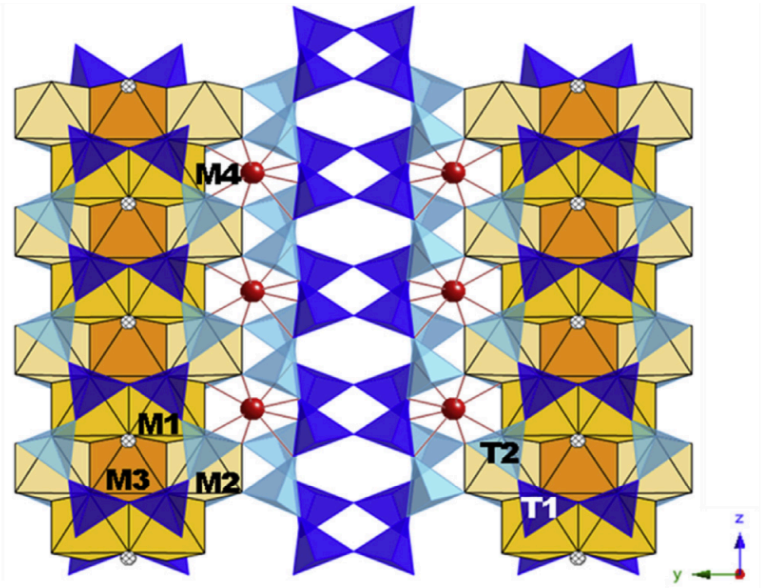

Figure 1.1.1 Structural model of monoclinic (C2/m) tremolite within the (100) plane. (Kong et al. 2018)

Amphibole is an important yet extremely complicated mineral group in terms of both the chemical composition and crystal structure. As a Ca-endmember amphibole, tremolite belongs to the double-chain silicate group with a monoclinic C2/m structure. It shares the same structures with other members in the same tremolite-ferro actinolite solid-solution join. The general chemical formula of amphibole is expressed as $A_{0\text{-}1}B_2C_5T_8O_{22}(OH, F, Cl)_2$. From the formula, a list of site occupation of an amphibole may be:

A = A site = Na, K, [ ], Ca, Li;

B = M4 site = Na, Li, Ca, Mn^{2+}, Fe^{2+}, Mg;

C = M1,M2,M3 sites = Mg, Fe^{2+}, Mn^{2+}, Al, Fe^{3+}, Mn^{3+}, Ti^{4+}, Li;

T = T1 and T2 sites = Si, Al, Ti^{4+}.

Some minor elements may be observed in the C site e.g. Cr^{3+}, Ni^{2+}, and Zr (Hawthorne and Oberti 2007; Robinson et al, 1982; Deer et al. 1997). The general configuration of amphibole is specified by two non-equivalent tetrahedral chains (e.g. T1 and T2) bounded together by strips of four M polyhedra (e.g. M1, M2, M3, and M4), resulting in what is called an "I-beam' structure (Sueno et al 1973).

The tremolite-actinolite-ferro-actinolite solid solution are commonly found in metabasites, gneiss, greenschist, and other calc-silicate rocks (Deer et al. 1997; Stoops et al. 2018). The International Mineralogical Association has defined the nomenclature of this series to be tremolite with Mg/(Mg+Fe2+) $\geq$ 0.90, actinolite with Mg/(Mg+Fe2+) = 0.50-0.90, and ferro-actinolite with Mg/(Mg+Fe2+) < 0.5. Therefore, the tremolite's general chemical composition ranges from $Ca_2Mg_5Si_8O_{22}(OH)_2$ to $Ca_2Mg_{4.5}\ Fe_{0.5}Si_8O_{22}(OH)_2$ (Deer et al. 1997; Gilbert et al. 1982).

Metamorphic rocks containing Ca-amphiboles are ubiquitous in a variety of continental and crustal setting. Thus, insights into its formation and behaviors at given P-T conditions are critical to understand the geologic processes upon the solidification. Ernst and Lui 1988 had synthesized the Ca-amphibole under known P-T ranges and specific oxygen fugacity. They determined that with the presence of Al- and Ti-rich phases amphibole would progressively be more calcium-rich as the temperature increases from 650 to 950 °C.

Through phase-equilibria and crystallographic studies, upon increasing the pressure, Al tends to replace Mg+Fe in the M2 site (Hawthorne 1981; Anderson and Smith 1995; Ernst and

Lui 1988). Experimental works show that Ca-amphibole is more enriched with Al_2O_3 as both pressure and temperature rises (Moody et al. 1983; Ernst and Lui 1988).

Comodi et al. (1991) have examined the high-P structures of tremolite using single-crystal X-ray diffraction and detected the decrease of the distance between the I-beams and the flattering of the tetrahedral chains. However, the silica tetrahedra show little to no modification up to 4.1 GPa (i.e. their experimental pressure range). The behavior of the M polyhedra and A site cations impact the compressible properties of each amphibole in the C2/m phase (Comodi et al. 1991; Yang and Prewitt 2000; Sueno et al 1973). Although previous studies have shown a similar compressibility along b and c axes, the compressibility along *a* is at least twice greater than that along *b* or *c* making A site to be the softest polyhedron among other polyhedra in tremolite (Yang and Prewitt 2000; Comodi et al. 1991). For M1, M2, and M3 of tremolite, cummingtonite, glaucophane, and pargasite, according to Comodi et al. (1991), the assigned cations in those sites will have prominent effects on the compressibility. Brown and Abramson (2016) also have found the increase in the single-crystal moduli (C_{11} and C_{13}) with the higher degree of A-site occupation, implying the more resistance to compression along the a*-direction.

The stability limit of amphibole in the mantle may be up to 3.8-4.0 GPa at 1000°C depending on the water and alkali contents (Niida and Green 1999; Fumagalli et al. 2009; Mandler and Grove 2016; Green et al. 2014). From the high-P single-crystal X-ray diffraction study of tremolite at 300 K, the crystal is stable up to at least 50 GPa at room-temperature conditions (Dera et al., personal communications).

1.2 Mid-lithospheric discontinuities

Cold and stable lithospheric cratons are usually formed in Archean and Early Proterozoic with a 200-240 km lithospheric root. Their structures, formation and evolution histories remain largely challenging to study (Yuan and Romanowicz 2010; Tharimena et al. 2016; Walter et al. 2012; Pollack 1986; Jordan 1988). Recently, various authors have studied these cratonic regions using different types of seismic techniques such as surface wave tomography and SRF. Seismic SRF is a powerful tool to detect the discontinuities in the Earth's interior. For the case of the MLD, seismologists have imaged a decrease in velocities between 80 to 100 km at various locations (Kumar et al 2012; Hopper and Fischer et al. 2015; Abt et al. 2010; Chen 2009). In some regions, the detected MLD depth can be up to 160 km or more, which might be caused by the use of different methods or local geological conditions (Hansen et al. 2015; Liu and Gao 2018).

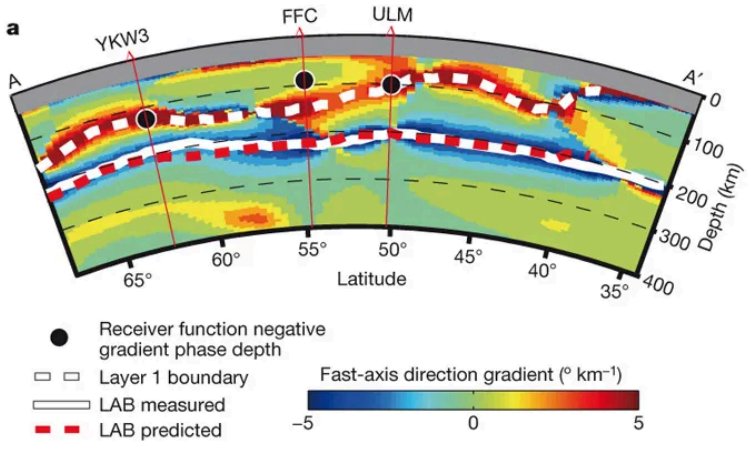

Figure 1.2.1 The white-dash line depicts the extreme change of the fast-axis anisotropy as the boundary between the top layer and layer underneath in which subsequentially interpreted to be the MLD. The white-solid line defines the gradient extreme of the lithosphere-asthenosphere boundary.

Yuan and Romanowicz (2010) have studied the azimuthal anisotropy beneath the craton and shown the change in orientation of the fast axis of anisotropy with depth. Two distinctive layers with a sharp gradient of the fast-axis direction have been detected through the SRF method. The shallow layer is a cold, chemically-depleted Archean lithosphere and underlain by a layer which appears to be a less-depleted thermal root. The boundary between these two layers is the highly anisotropic MLD as depicted as on Figure 1.2.1 with a white-dash line. The authors have attributed the observed anisotropy change primarily to the compositional layering under the craton. However, as pointed out by Selway et al. (2015), geochemical depletion in terms of Mg# change is not enough to cause 3-10% velocity drop across the MLD. Moreover, the lack of information on the dip of the axis of symmetry also affects our understanding the source of the seismic anisotropy.

Due to the wide distribution of MLD over the globe, there have been several attempts to explain the MLD with a single universal mechanism. For example, Kumar et al. (2012) and Thybo (2006) combined the seismic data, heat flow data, and xenolith thermobarometry, and they proposed the partial melting hypothesis as the cause of the MLD. However, this theory may not be able to explain the occurrence of the MLD. As shown in Figure 1.2.2, the lithosphere that would undergo partial melting at the MLD depth must be water-saturated and chlorite-rich, which is considered to be an anomalous composition within the craton (Till et al. 2012; Griffin et al. 2009; Selway et al. 2015).

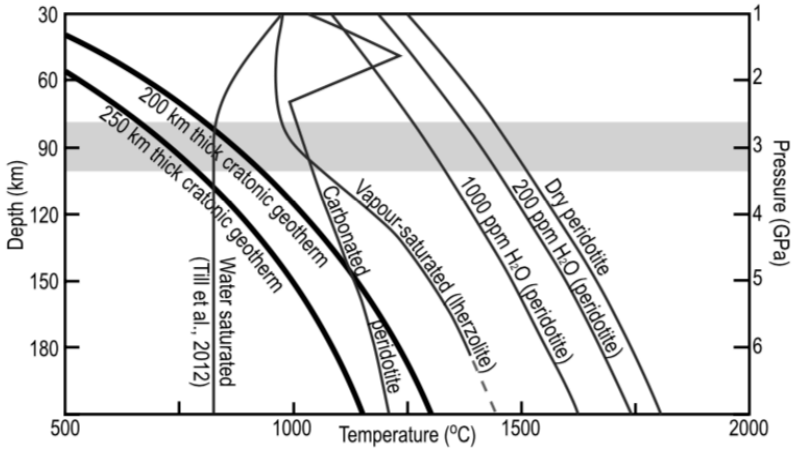

Figure 1.2.2 The experimental solidus acquired (Dasgupta 2013; Dasgupta and Hirschmann 2010; Green et al. 2010; Hirschmann 2006) from Selway et al. (2015) showing the standard cratonic geotherm that crosses the water-saturated solidus at the depth of the MLD. This phenomenon implicates that the partial-melting melting would occur at this depth if the craton is water-saturated.

Other possible mechanisms include grain boundary sliding (Karato 2012), radial and azimuthal seismic anisotropy (Rychert and Shearer 2009; Ford et al. 2016; Liu and Gao 2018), and production of low-velocity minerals like amphiboles and phlogopite by metasomatism (Liu and Gao 2018; Griffin et al. 2004; Foster et al. 2014; Hansen et al. 2015). Although the attempt to explain the MLD with a single universal mechanism seems to be not successful (Selway et al. 2015), the existence of low-velocity hydrous minerals such as amphiboles, phlogopite, and carbonetite is believed to be the most common cause or partial cause of the MLD over the world. This is also the primary motivation of this study.

1.3 Hydrous minerals and Metasomatism

Water determines the physical and chemical characteristics of the Earth's system from the atmosphere to its complex interiors. The transportation of water from the surface or the shallower region can occur at an active convergent margin where the oceanic crusts are recycled and sink down to the deep mantle (Zhu and Yang 2016; McInnes et al. 2001). The sinking slab pertaining hydrous minerals can reach the depth of at least 660 km (Yong et al. 2019; Bina et al. 2001; Kirby et al. 1996) and release water at any possible depth, depending on the mineral's stability. Sufficient amounts of the releasing water, combining with the effects from pressure and temperature, will cause the partial melting of the mantle, modify the mantle's rheology, trigger the deep earthquake, and lead to metasomatic processes (Bina et al. 2010; Zhu and Yang 2016).

Hydrous minerals such as amphibole, chlorite, serpentine minerals, phlogopite and NAM contain different amounts of water in their structures. For example, minerals in amphibole group are constituted by water for approximately 2-4%. Phlogopite's water content can reach over 5%, while serpentine's water content can be up to 13% (Carlson and Miller 2003). Comparing the anhydrous phases, hydrous minerals cause the reduction in the seismic velocities (Selway et al. 2015). Therefore, the occurrence of hydrous minerals with the relevant P-T condition can potentially generate the zone or layers of negative velocity gradient.

Metasomatism generally refers to the dissolution of one mineral at the same time as the replacement of another minerals, e.g. amphibole, chlorite, and quartz as a result of the introduction of a new material (Ran et al. 2019). This alteration process may occur in the mantle wedge because of the dehydration of the subducted slabs (Johnson et al. 1996; Ozawa

1988; Neal and Taylor 1989). It could also occur in the subcontinental lithosphere that has not been associated with the convergent plate boundary over billions of years due to the remobilization of elements (Frost 2006). Hydrous minerals appear to have lower seismic velocities compared to their anhydrous counterparts (Selway et al. 2015; Hacker et al. 2003; Frost 2006; Schmidt and Poli 1998), making them excellent candidates to account for low velocity regions in the Earth's interior. In the case of amphiboles and phlogopite, they are produced from the reactions of ascending melts or H_2O-CO_2-rich fluids with mantle peridotite, thus are enriched in incompatible elements (e.g. K, Rb, Sr, Ti, U, LREE) (Roden and Murthy 1985; Bailey 1982; Menzies et al. 1987; Selway et al. 2015; Johnson et al. 1996). Pirard and Hermann (2015) had determined the stability of alkali amphibole in metasomatized dunite using the piston-cylinder apparatus and observed amphiboles in all experiments at 2.5, 3.5, and 4.5 GPa with various temperature ranges. The amphibole has been found to be an abundant phase at 3.5 GPa, consistent with studies from Mandler and Grove (2016), Selway et al (2015), and Waters and Erlank (1988) etc. as shown in Figure 1.3.1.

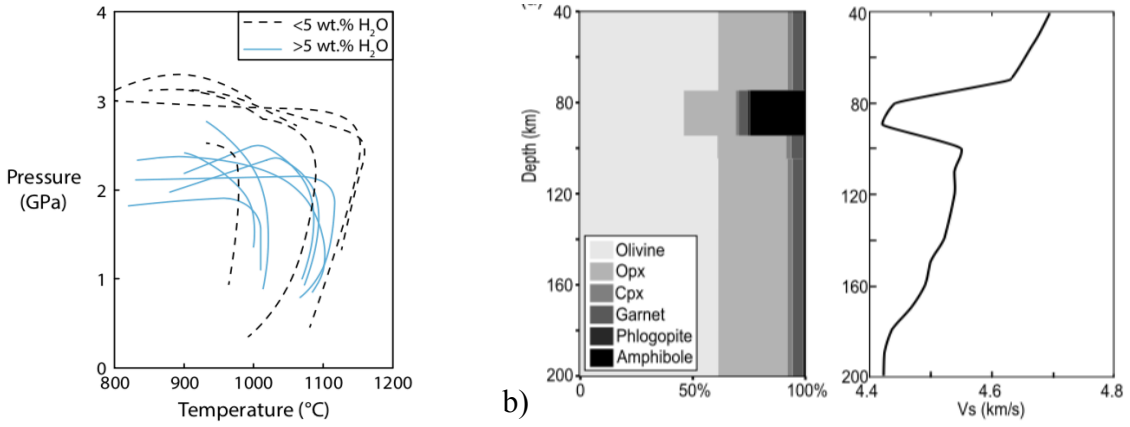

Figure 1.3.1 (a) Experiments on amphibole stability from Kushiro (1970), Green (1973), Millhollen et al. (1974), Mysen and Boettcher (1975), Mengel and Green (1989), Wallace and Green[a)] (1991), Niida and Green (1999), Grove et al. (2006), Fumagalli et al. (2009), and

Tumiati et al. (2013), after Mandler and Grove (2016). (b) Modal compositions of the lithospheric mantle with 25% amphibole from 75 km to 90 km and 1% phlogopite corresponding to the shear wave velocity reduction (Selway et al. 2015).

1.4 Single-crystal Elasticity

The elastic properties of mantle mineral are crucial guides to probe the physical and chemical characteristics of the deep interior. Elasticity of these minerals holds such insights into understanding the seismic observation, geodynamic model, and chemical constraints of the mantle. Elasticity of a mineral is a function of pressure and temperature because it pertains the information about the change in volume of a mineral at a given state. Therefore, it allows the interpretation about the minerals and chemical properties at that condition (Mainprice 2007; Birch 1952; Fan et al 2015; Angel et al. 2009). The elasticity of a single-crystal mineral can be obtained through the measurement of the acoustic velocity. These waves are characterized into compressional or Vp and shear or Vs (Angel et al. 2009) on the basis of the particle motion and the wave propagation. The velocity of an anisotropic single-crystal mineral depends on the orientation of the crystal. Consequently, the accurate measurement of the orientation of the crystal plays such a significant role in determining the elastic tensor and other thermoelastic parameters associating with the directional-dependence velocities.

1.5 Anisotropy

Tremolite exhibits the maximum anisotropy for the Vp in the X-Z plane and most isotropic in the Y-Z plane according to the Impulsive Stimulated Light Scattering (ISLS) data obtained

by Brown and Abramson (2016) at ambient condition. They measured nine varieties of amphiboles in the experiments and compared the data with their clinopyroxene equivalents. For the Vs, tremolite appears to be the most anisotropic amphibole among all, with Vs varying from 3.7 km/s to 5.2 km/s. Tremolite's anisotropic properties were analyzed along with diopside's data obtained from Isaak et al. (2006). The results are uniformly consistent with other composition of amphiboles and their pyroxene counterparts in which tremolite is more anisotropic than diopside owing to small moduli associated with a*- direction (C_{11}, C_{12}, C_{13}, C_{55}, and C_{66}). Due to the vacancy or the partially-filled A site of tremolite, this phenomenon allows more strain in the a-axis direction (Brown and Abramson 2016).

Under the simple shear, amphiboles usually behave aligned its (100) pole subnormal to the shear plane and [001] axis subparallel to the shear direction (Ko and Jung 2015; Kim and Jung 2019). The dehydration of amphibole in the presence of olivine occurred in the metasomatized mantle is controlled by the following reaction (Frost 2006):

$$Ca_2Mg_5Si_8O_{22}(OH)_2 + Mg_2SiO_4 = 2CaMgSi_2O_6 + 2.5Mg_2Si_2O_6 + H_2O$$

Tremolite Olivine Clinopyroxene (Diopside) Orthopyroxene Fluid

The stability field of amphiboles can be extended to higher pressure and temperature condition by the substitutions of cations e.g. K, Ti, or possibly Cr into the amphibole structure (Yong et al. 2019; Mandler and Grove 2016). As the primary dehydration product, clinopyroxenes form completely different deformation texture from amphiboles with the [001] direction aligning parallel with the shear direction with the [010] perpendicular to the shear plane (Bascou et al. 2001). The stronger anisotropy observed in amphiboles (Ca-end member tremolite) compared with clinopyroxenes (Ca-end member diopside), combined with the different deformation mechanisms (Isaak et al. 2006; Brown and Abramson 2016), provide a

possible alternative explanation for the anisotropy change across the MLD (Yuan and Romanowicz, 2010). This is another motivation of this study.

2. Methods

2.1 Diamond Anvil Cell (DAC)

The DACs used in this study are both SYM60 with the culet size of 300 and 350 microns. The typical thickness of the gasket is about 45-55 microns with a sample chamber of, approximately, 150 microns in diameter. A single-crystal tremolite is placed within the DAC sample chamber with two rubies serving as pressure calibrants. The 4:1 methanol-ethanol mixture is used as a pressure-transmitting medium because it will remain at least hydrostatic up to 10.4 GPa (Piermarini et al. 1973; Hazen and Downs 2000). An increase of the load onto the diamond anvils by tightening the screws generates the high-pressure condition (Miletich et al. 2000; Hazen and Downs 2000). The pressure will be determined using ruby fluorescence (Mao et al. 1986)

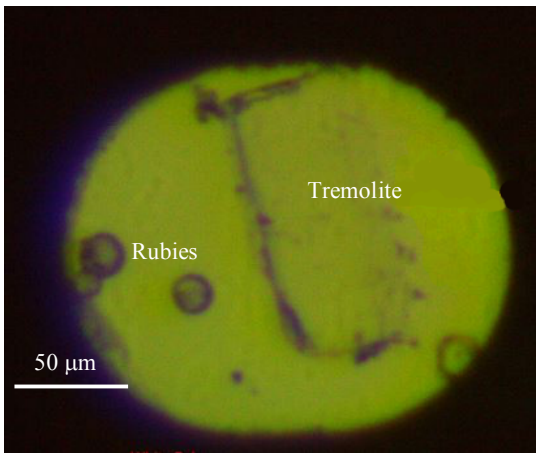

Figure 2.1.1 shows the tremolite sample loaded in DAC sample chamber. The (1100) face of the tremolite was placed closed to two rubies inside the gasket with the alcohol mixture as the

pressure transmitting media loaded. The DAC is completely assembled and ready for the experiment.

2.2 Sample Preparation

The lateral dimension of the single crystals used for DAC experiments were less than 2/3 to 3/4 of the sample chamber (Miletich et al. 2000; Hazen and Downs 2000). The experiments were performed on a tremolite sample with a chemical formula of $Na_{0.09}(Ca_{1.98}Na_{0.02})(Mg_{4.735}Al_{0.24}\ Mn_{0.01})\ (Si_{7.72}Al_{0.28})O_{22}(OH)_{2.}$. A think plate (~20 microns) with orientation (110) was picked for the Brillouin measurements without polishing due to the perfect cleavage of tremolite. Crystals with other orientations were polished down to the thickness of 20-30 microns. The clean and flat polished crystals were further analyzed using single-crystal X-ray Diffraction to obtain their orientations.

2.3 Electron Probe Microanalysis (EPMA)

We used the JEOL 8200 Electron Microprobe Facility hosted at the Institute of Meteoritics at UNM to analyze the chemical compositions of the two selected tremolite crystals. The selected crystals were cleaned and then carbon-coated with a carbon evaporation source. The data were collected at 15-kV accelerating voltage and 20-nA beam current. The typical quantitative analysis of elements from silicates minerals are expressed in terms of elemental mass concentration or weight percent of oxides (Hao et al. 2019; Reed 2005). The calculated chemical formula of the tremolite of this study is $Na_{0.09}(Ca_{1.98}Na_{0.02})(Mg_{4.735}Al_{0.24}\ Mn_{0.01})\ (Si_{7.72}Al_{0.28})O_{22}(OH)_{2.}$ The chemical analysis is shown in Table 2.1.

2.4 X-ray Diffraction (XRD)

Single-crystal XRD experiments were performed on the two polished tremolite crystals in the DACs at the Hawaii Institute of Geophysics and Planetology, University of Hawaii at Moana. The diffraction images at various scattering angles were collected using a Bruker D8 Venture XRD diffractometer with Helios focusing optics and Photon II detector at 300K. Both wide-scan and 1°/step step-scan were captured. Then, these images were processed via the Bruker APEX III software. The plane normal of the two polished tremolite crystals are (-0.831, 0.482, 0.279) and (0.970, -0.022, -0.244). The unit cell parameters determined from the two tremolite crystals are a =9.7897±0.0025 Å, b=18.0172±0.0021 Å, c=5.2618±0.009 Å, α= ɣ=90°, and β=104.8890±0.015 ° The calculated ambient density of tremolite is 3.000 ±0.34 g/cm^3

Table 2.1 Raw chemical composition of Tremolite from the EPMA analysis

Composition	(%)	Element	(Wt%)
MgO	24.4615	Mg	14.7509
Al_2O_3	0.927935	Al	0.491106
Na_2O	0.051637	Na	0.038307
SiO_2	58.2018	Si	27.2053
CaO	13.7774	Ca	9.84661
FeO	0.02943	Fe	0.022876
MnO	0.084026	Mn	0.065074
Cr_2O_3	0.061102	Cr	0.04186
		Y	0
		O	45.1328
Total	97.5947		97.5947

2.5 Single-Crystal Brillouin Spectroscopy

The Vp and Vs of tremolite crystals along 3 different crystallographic directions are measured using Brillouin spectroscopy at 0,1.6 ± 0.12, 2.6 ± 0.2, 3.3 ± 0.03, 5.4± 0.1, and 7.7± 0.1 GPa at 300 K in the Mineral Physics laser spectroscopy lab at UNM. The single mode 532-nm laser was used as the light source. The calibrated scattering angle is 50.77±0.06º. The plate spacing used for all Brillouin measurements is 6.6 mm. The 6-path tandem Fabry-Perot interferometer is used to obtain high resolution Brillouin frequency shifts (Sandercock, 1982). One Vp, and one or two Vs are observed in each Brillouin spectrum. At each pressure, the velocities are determined at 24 Chi angles along the 360º azimuth to prevent any geometric errors. A sample Brillouin spectrum is shown in Figure 2.5.1

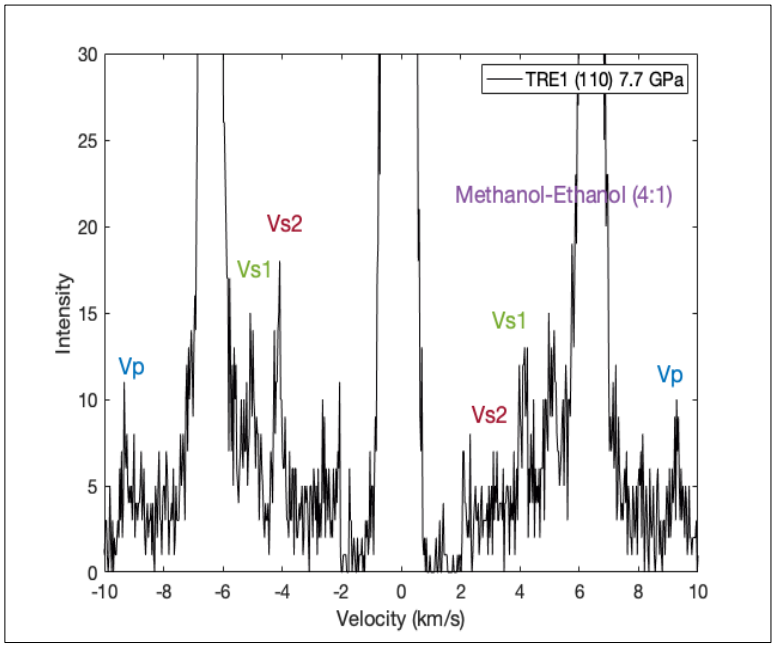

Figure 2.5.1 A typical Brillouin spectrum of single-crystal tremolite at 300K and 7.7 GPa

Due to the quality issues of the spectra obtained from the (-0.831, 0.482, 0.279) and (0.970, -0.022, -0.244) orientations, this study only used the velocities collected within the (110) cleavage plane for data evaluation.

2.6 Derivation of the single-crystal elastic properties at high-pressure condition

Monoclinic tremolite has 13 independent C_{ij}s which are the abbreviated elasticity tensor C_{ijkl} under Voigt notation. They can be obtained through the inversion of the Christoffel equation (Musgrave 1970; Jackson et al. 2007; Mainprice 2015; Christoeffel 1877):

$$\mathrm{Det}|C_{ijkl}n_j n_l - \rho V^2 \delta_{ik}| = 0 \quad (1)$$

n represent the phonon direction. ρ is the density. $\delta_{ik}|$ is the Kronecker delta. V is sound velocity along the probed phonon direction.

The Voigt-Ruess-Hill averaging scheme (VRH) are utilized to determine the aggregate elastic properties of tremolite from the C_{ij}s, including adiabatic bulk modulus (Ks), shear modulus (G), Vp, and Vs. (Hill 1963).

The high-pressure single-crystal elastic properties (Vp, Vs, Ks, G, and C_{ij}s) and the densities of tremolite at each experimental pressures are calculated through the least-square inversion of Christoffel equation with an assumed fake density. The calculated parameters will later be fitted with to the third-order finite strain equation of state to get the true densities under high pressures and also the pressure derivatives of Ks and G. The obtained true densities will then be used to update the single-crystal elastic moduli at high-pressure condition. (Davies 1974; Hao et al. 2019).

A few anisotropy indices are used to evaluate the anisotropy of tremolite at high-pressure condition. The universal anisotropy index (A^u) provides a measurable index to evaluate the anisotropy for crystals with arbitrary symmetry. The value of A^u is 0 for isotropic media, and increases with the differences between Voigt and Reuss bounds (Ranganathan and Ostoja-Starzewski 2008; Kube 2016). A^u was defined as following:

$$A^{u} = \frac{k^V}{k^R} + 5\frac{\mu^V}{\mu^R} - 6 \quad (2)$$

The A^{Vp} and A^{Vs} anisotropy is derived using equation (3) and (4) to show the maximum Vp and Vs difference along different directions:

$$A^{Vp} = \frac{Vp_{max} - Vp_{min}}{Vp_{VRH}} \quad (3)$$

$$A^{Vs} = \frac{Vs_{max} - Vs_{min}}{Vs_{VRH}} \quad (4)$$

in which Vp_{VRH} and Vs_{VRH} are the velocities derived from the Voigt-Reuss-Hill averaging scheme (Hill 1963). D^{Vs} is the polarizational Vs anisotropy or Vs-splitting anisotropy, which depends on the maximum velocity difference of two shear waves that are propagating in the same direction with orthogonal polarization:

$$D^{Vs} = \frac{|V_{s1} - V_{s2}|_{max}}{Vs_{VRH}} \quad (5)$$

3. Results and Discussion

3.1 Equation of state of Tremolite

a. Unit cell parameters at ambient condition

At 300K, the unit cell volume obtained from single-crystal XRD is 901. 32 ± 0.18 $Å^3$. Comodi et al. (1991) and Ott et al. (2020) measured the ambient unit cell volume of closet end-member tremolite, which are determined to be 905.76 $Å^3$ and 904.9 $Å^3$, accordingly. The differences in the unit cell volume are likely caused by the compositional difference between the samples used in those studies. For the sample of this study, as Al and Mn substitute for Mg in the M sites, Si is also replaced by Al in the tetrahedral chains. Moreover, the A site is also occupied by Na, which is different from the vacancy of the A site from previous studies. The chemical composition of tremolite from Ott et al. (2020) were close to the ideal end-member, which was Ca_2Mg_5 $Si_8O_{22}(OH)_2$, because of a minimal replacement of Mg^{2+} by Fe^{2+}(Ott and William 2020). The EPMA analysis of the tremolite sample from Comodi et al. (1991) also indicated that their sample was $Ca_2(Mg_{4.95}Fe^{2+}_{0.05})$ $Si_8O_{22}(OH)_2$.

The unit cell volume at ambient condition from Peng and Mookherjee (2020) using the determined LDA and GGA approximation were 887.1 $Å^3$ and 958.4 $Å^3$, respectively. Their computational studies on the thermoelastic parameters also assumed the composition of Mg-end member.

The value determined in this study is within the bounds given by LDA and GGA. The ambient unit cell volume of this study differs less than 0.5 % from Comodi et al. (1991) and Ott et al. (2020) as specified in Table 3.1

Table 3.1 Comparison of normalized volume (V/V_0) at 300 K of this study with previous publication

This study		Peng and Mookherjee (2020)				Comodi et al. 1991		Ott J. (2020)	
Pressure (GPa)	V/V_0	Pressure (GPa)	**LDA** V/V_0	Pressure (GPa)	**GGA** V/V_0	Pressure (GPa)	V/V_0	Pressure (GPa)	V/V_0
0.001	1.0	0.001	1	0.001	1	0.03	1	0.001	1
1.00	0.989	0.65	0.992	1.37	0.981	0.79	0.991	1	0.985
2.00	0.979	1.61	0.980	3.07	0.960	1.23	0.982	1.9	0.977
3.00	0.969	2.65	0.970	5.05	0.940	1.83	0.976	2.5	0.969
4.00	0.961	3.75	0.958	7.33	0.918	2.73	0.967	3.7	0.955
5.00	0.952	4.94	0.947	9.97	0.890	2.93	0.964	4.9	0.945
6.00	0.945	6.22	0.936			3.28	0.963	5.9	0.940
7.00	0.938	7.58	0.924			3.56	0.962	7.2	0.926
8.00	0.931	9.05	0.913			3.53	0.961	8.8	0.914
						4.10	0.958	9.4	0.914
								10	0.910
								10.3	0.910
								11.1	0.905
								11.6	0.900
% Differences of volume at 300 K from this study		2.41%		4.12%		0.50%		0.40%	

b. High-pressure Normalized V/V_0

Sound velocity measurements can be utilized to calculate the density and unit cell volume at high-P conditions through finite-strain equation of state (Davies & Dziewonski 1975). Therefore, it is worth to compare the V/V_0 values derived from the Brillouin experiments in this study with previous computational study and XRD experiments. The comparison between this study and previous studies are shown in Figure 3.1.1.

Previous studies are in agreement with each other. However, this study is different. The sample is less compressible compared with previous studies. For example, the V/V_0 determined in high-pressure x-ray diffraction study of Comodi et al. (1991) deviates from this

study by 0.8% upon reaching 4 GPa. The V/V_0 values from the LDA method differ from this study by 6% which is expected. These discrepancies are primarily caused by the compositional differences. The substitution of Al in the tetrahedral site and the Na occupancy in the A site both tend to stiffen the crystal structure (Brown and Abramson et al. 2016; Nestola et al. 2012). The amount of substitution of Ca in the M4 site also affects the compressible properties in the c*-direction (Yang and Prewitt 2000). Even though the sample from Ott J. (2020) and Comodi et al. (1991) possessed a higher extent of Ca, the effect along a*-direction due to the occupancy in the A site is approximately twice greater than that of c*-direction. Therefore, with the occupancy of the A site of tremolite in this study, it is less compressible than those in previous studies, which expressed through its higher V/V_0 values at high-pressure conditions.

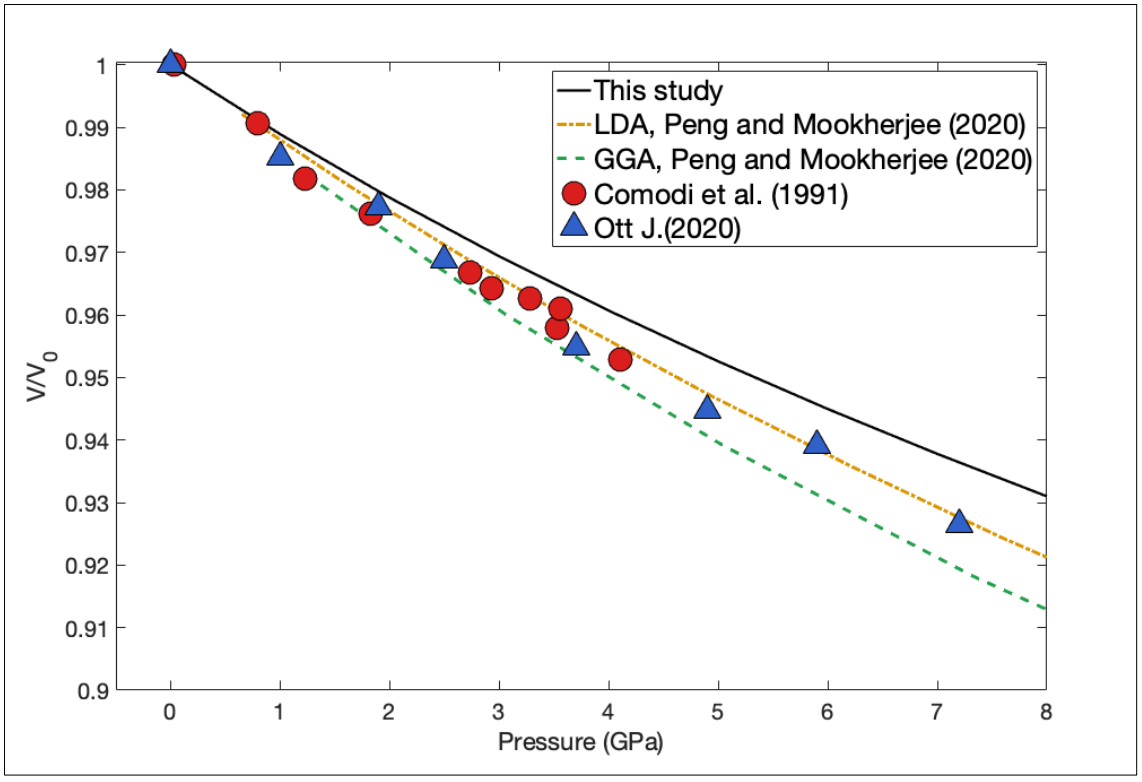

Figure 3.1.1 Normalized volume (V/V_0) of single-crystal tremolite determined from the Brillouin experiments in this study and the comparison with previous studies (Peng and Mookherjee 2020; Comodi et al. 1991; Ott J. 2020).

3.2 Elastic properties of tremolite at ambient condition

a. Comparison of Ks and G with previous studies

The ambient Ks, G, and C_{ij}s of tremolite determined in this study are shown in Table 3.2. The Ks calculated using LDA and GGA approximations are 78.5±10 GPa and 66.3±10 GPa, respectively (Peng and Mookherjee, 2020). Both are smaller than the ambient Ks of 86±6 GPa determined in this study. The G of 58.0±10 GPa determined from LDA approximation is similar to 59±4 GPa measured in this study. The Ks and G of tremolite measured in Brown and Abramson (2016) are 78 GPa and 58 GPa, which agree well with the LDA approximation. The higher Ks measured in this study is caused by the stiffening effects due to the element substitutions in the tremolite structure. It also agrees with the higher V/V_0 at elevated pressure as depicted in Figure 3.1.1.

b. Comparison of C_{ij}s with previous studies

Tremolite amphibole has a monoclinic C2/m structure with 13 independent C_{ij}s. A least square inversion of the Christoffel equation was used to calculate the best-fit values for the 13-independent C_{ij}s at ambient condition (Weidner and Carleton 1977). The comparison of the C_{ij}s between this study and previous studies are shown in Figure 3.2.1 and Table 3.2. The

measured velocities associated with the velocity model predicted by the C_{ij} model of tremolite are shown on Figure 3.2.1.

At ambient condition, C_{11} of this study is identical to the C_{11} calculated from the LDA results of Peng and Mookherjee (2020), which are 109±2 and 109.4, respectively. The C_{22} of this study is higher than the LDA approximation in Peng and Mookherjee (2020) and Brown and Abramson (2016) values, which are 202±4, 191.5, and 191.6 GPa, respectively. The C_{33} from Brown and Abramson (2016) is the largest elastic constants, whereas C_{33} of this study is less than C_{22}, which is consistent with the LDA and GGA approximation. The C_{66}, C_{12}, C_{25}, C_{35}, and C_{46} of this study fall between the bound of LDA and GGA results. The C_{12} and C_{23} of this study are higher than those of the LDA and GGA approximation. Overall, all the C_{ij}s of this study are in reasonable agreement with the C_{ij}s determined from these two previous studies.

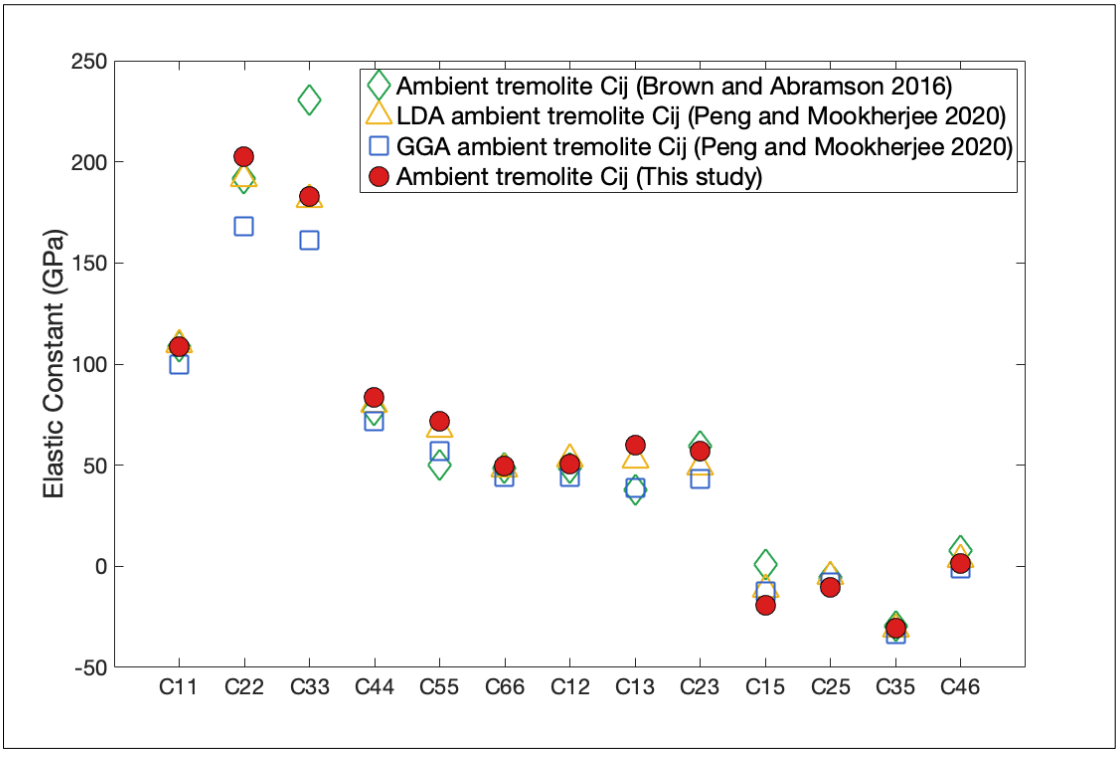

Figure 3.2.1 The 13 independent elastic moduli of tremolite amphibole at ambient condition.

Brown and Abramson (2016) studied the compositional influence on the elastic moduli at ambient conditions. Al and Fe contents were shown to affect the elastic properties significantly. C_{11}, C_{12}, C_{13}, C_{22}, C_{44}, C_{55}, and C_{66} increase with Al content, and decrease with Fe content. This compositional effect is consistent with the larger value of C_{12}, C_{13}, C_{44}, C_{55}, and C_{22} of this study than those from Peng and Mookherjee (2020). The tremolite sample used in this study has the Al substitution in both M sites and silica tetrahedral site while Peng and Mookherjee (2020) assumes the ideal Mg end-member composition. The C_{44}, C_{13}, and C_{12} also increases with the higher occupancy of Na and K in the A sites. This compositional dependence provides the explanation for the C_{44}, C_{13}, and C_{12} of this study as they are larger than those from Peng and Mookherjee (2020). These values agree with the fact that the tremolite of this study has Na in the A site, while Peng and Mookherjee (2020) assume their A site to be vacant. The C_{25} and C_{15} of this study agrees well with C_{25} and C_{15} from Brown and Abramson (2016) and Peng and Mookherjee (2020) as they are close to 0. According to Brown and Abramson (2016), C_{46} reduces with higher Al content. Thus, the C_{46} of this study is slightly smaller than those of Peng and Mookherjee (2020) and Brown and Abramson (2016).

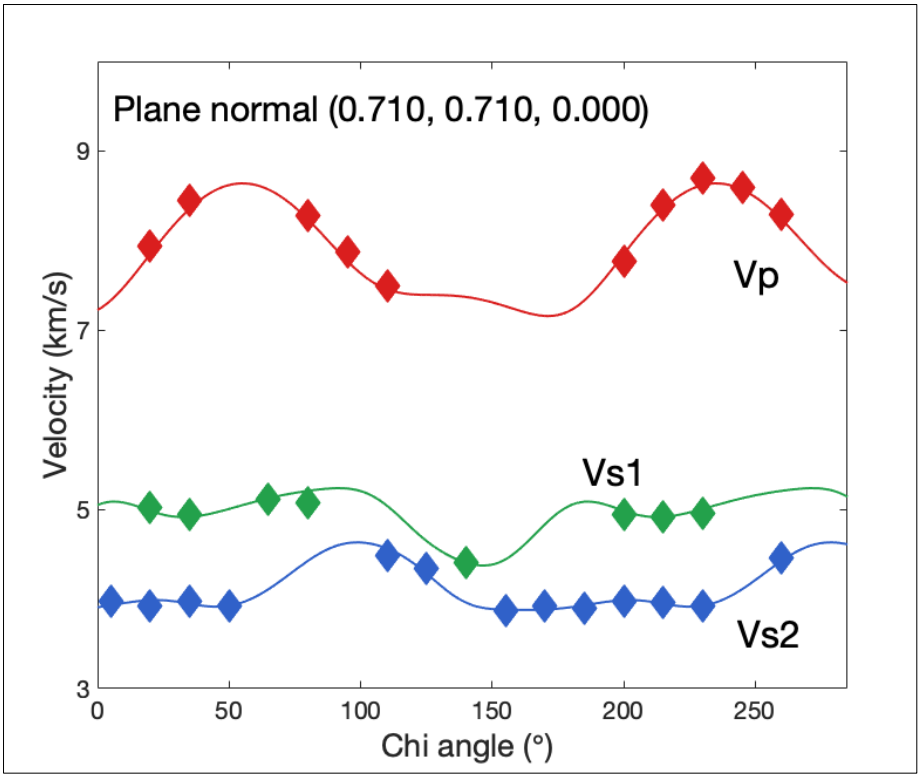

Figure 3.2.2 Measured velocity data of the single-crystal tremolite as a function of the chi angles for (0.710, 0.710, 0.000) orientations at ambient condition. Solid lines are the acoustic velocities calculated from the best-fit single-crystal elasticity model; Open symbols are the experimentally determined velocities. Errors are within the size of the symbols. The RMS error is 65.8 m/s.

C_{11}, C_{13}, C_{22}, C_{44}, and C_{55}, determined in this study is larger than from that of Brown and Abramson (2016) because the tremolite used in this study has less Fe and more Al content.

Table 3.2. Summary of tremolite's elastic properties from this study and previous publication

Elastic Moduli	**Brown and Abramson (2016)**	**Peng and Mookherjee (2020)**		**This study**
	0 GPa, 300K from ISLS experiments	0 GPa, 300K from LDA approximation	0 GPa, 300K from GGA approximation	0 GPa, 300 K from Single-Crystal Brillouin experiment
	r = 3.038 g/cm^3	r = 3.04 g/cm^3	r = 2.81 g/cm^3	r = 3.00 g/cm^3

C_{11} (GPa)	108.6	109.4	100.0	118±2
C_{22} (GPa)	191.6	191.5	168.2	188±4
C_{33} (GPa)	230.8	181.2	161.4	181±2
C_{44} (GPa)	77.0	80.0	71.8	79±2
C_{55} (GPa)	50.0	67.6	57.0	64±2
C_{66} (GPa)	48.6	47.9	44.3	47±3
C_{12} (GPa)	48.4	53.1	44.2	58±2
C_{13} (GPa)	37.7	52.6	38.8	55±3
C_{23} (GPa)	59.2	49.1	43.0	42±2
C_{15} (GPa)	1.0	-11.6	-12.2	-10±2
C_{25} (GPa)	-5.6	-5.1	-8.0	-5±2
C_{35} (GPa)	-29.6	-31.3	-33.5	-27±2
C_{46} (GPa)	7.9	3.5	-1.2	2.3±0.4
Ks^{VRH}(GPa)	78	78.5	66.3	86±6
G^{VRH}(GPa)	58	58	NA	59±4
Vp (m/s)	7.38	7.24	7.07	7.37±0.1
Vs (m/s)	4.45	4.34	4.29	4.42±0.1
RMS (m/s)	40	NA	NA	65.8

c. Comparison of ambient velocity with other upper mantle minerals

The stability and geochemical constraints from mantle xenoliths suggested that the upper mantle primarily consists of olivine, clinopyroxene, orthopyroxene, and garnet (Frost D.J. 2008). Tremolite amphibole can also coexists with these mantle phases within its stability field before encountering the dehydration processes at P-T condition exceeding 3-4 GPa and 1100-1200 ºC (Mandler and Grove 2016; Green et al. 2014). We can compare the velocities of tremolite and other upper mantle minerals at ambient condition. Tremolite shows the smallest Vp and Vs comparing to olivine, clinopyroxene, and orthopyroxene as shown in Table 3.3. The lower values of Vp and Vs of tremolite are expected. Hydrous minerals usually have

slower velocities compared to other anhydrous phases at the same P-T conditions (e.g., Hackers et al 2003; Selway et al. 2015).

Table 3.3 Velocity of mantle minerals at 300 K and 0 GPa.

References	Vp (km/s)	Vs (km/s)
Tremolite (This study)	7.37 ± 0.1	4.42 ± 0.1
Clinopyroxene (Ming et al. 2019)	8.13 ± 0.4	4.70± 0.3
Orthopyroxene (Zhang and Bass 2016)	8.06 ± 0.3	4.80 ± 0.2
Olivine (Zhang and Bass 2016)	8.33 ± 0.03	4.80 ± 0.03
Clinopyroxene (Sang and Bass 2014)	8.06	4.72

At ambient condition, the average of Vp of the most common mantle minerals are higher that the Vp of tremolite of this study by 10%. The average of Vs of the most common mantle minerals are higher that the Vs of tremolite of this study by 8%. The Vp and Vs of common mantle minerals, amphibole group, and tremolite for each study are shown in Figure 3.2.3 and 3.2.4, respectively.

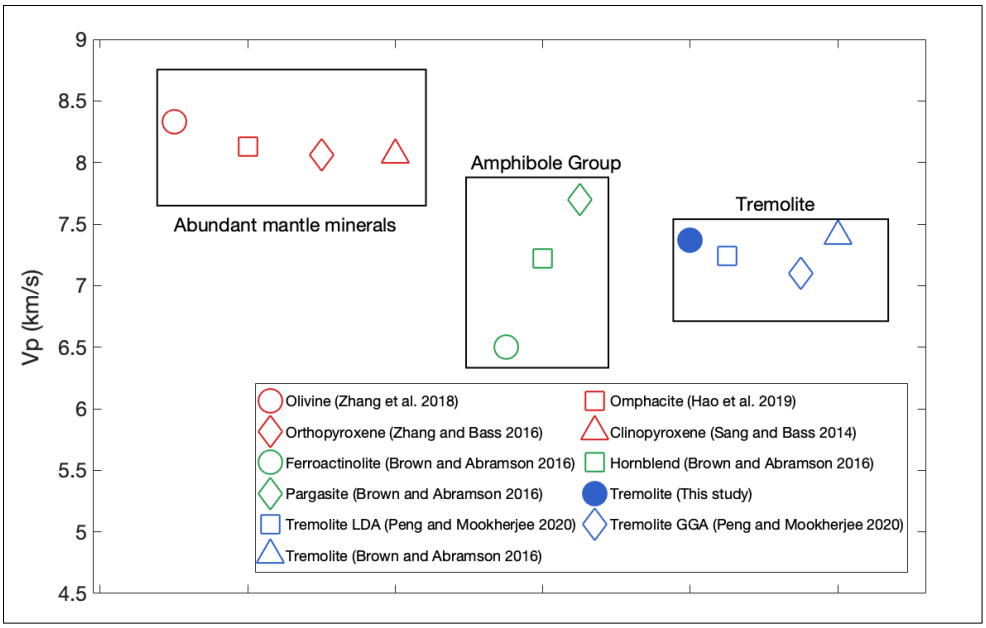

Figure 3.2.3 Vp of typical minerals compared with tremolite in this study

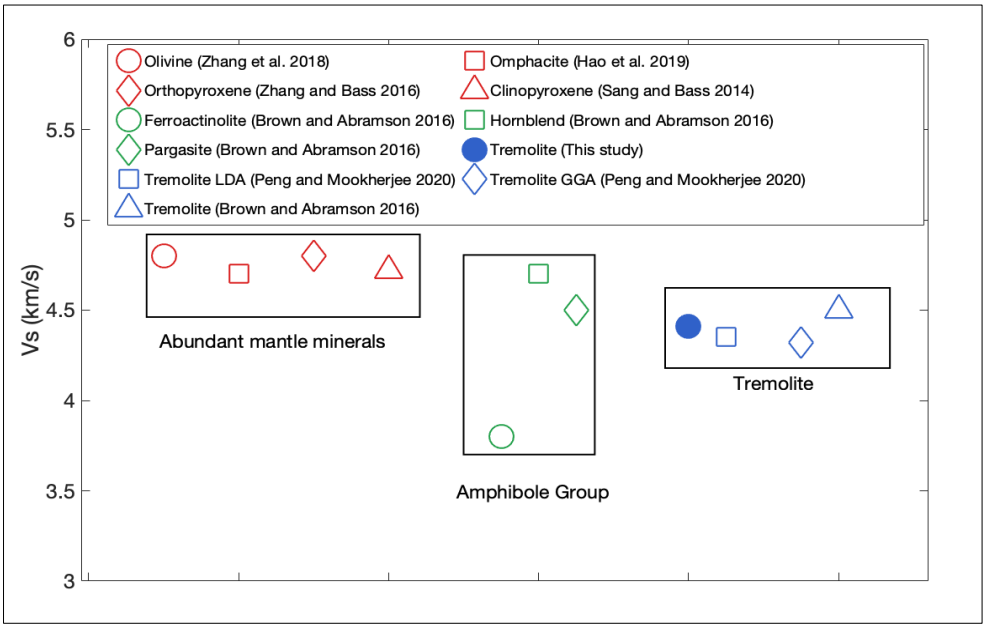

Figure 3.2.4 Vs of typical minerals compared with tremolite in this study

3.3 Elastic properties of tremolite at high-pressure conditions

a. Aggregate elastic properties at high-pressure condition (Ks, G, Vp, and Vs)

The best-fit high-pressure elastic properties at 300 K determined in this study are plotted in Figure 3.3.1 and listed in Table 3.4. The pressure derivatives of Ks and G are 7.5±3 and 1.9±1, respectively. Peng and Mookhergjee (2020) reported their pressure derivatives of Ks and G as 5.9 and 1.3, respectively. Ks and G values increases with pressure, suggesting that tremolite stiffens as the pressure increases.

The Ks and G of this study is significantly higher than all the values presented in Peng and Mookherjee (2020). They are in slightly better good agreement with the LDA approximation from Peng and Mookherjee (2020) compared with the GGA approximation, which is expected. In terms of Vp and Vs, this study is consistent with Peng and Mookherjee (2020) that the Vp increases at a much faster rate compared to Vs. Both Vp and Vs of this study are significantly faster than the Vp and Vs from Peng and Mookherjee (2020) throughout the investigated pressure range. The large discrepancy between this study and previous studies suggests that either the composition has a large effect on the high-pressure aggregate elastic properties, or the fact that the data presented in this study is not well-constrained because of the use of only velocity data along (110) orientation.

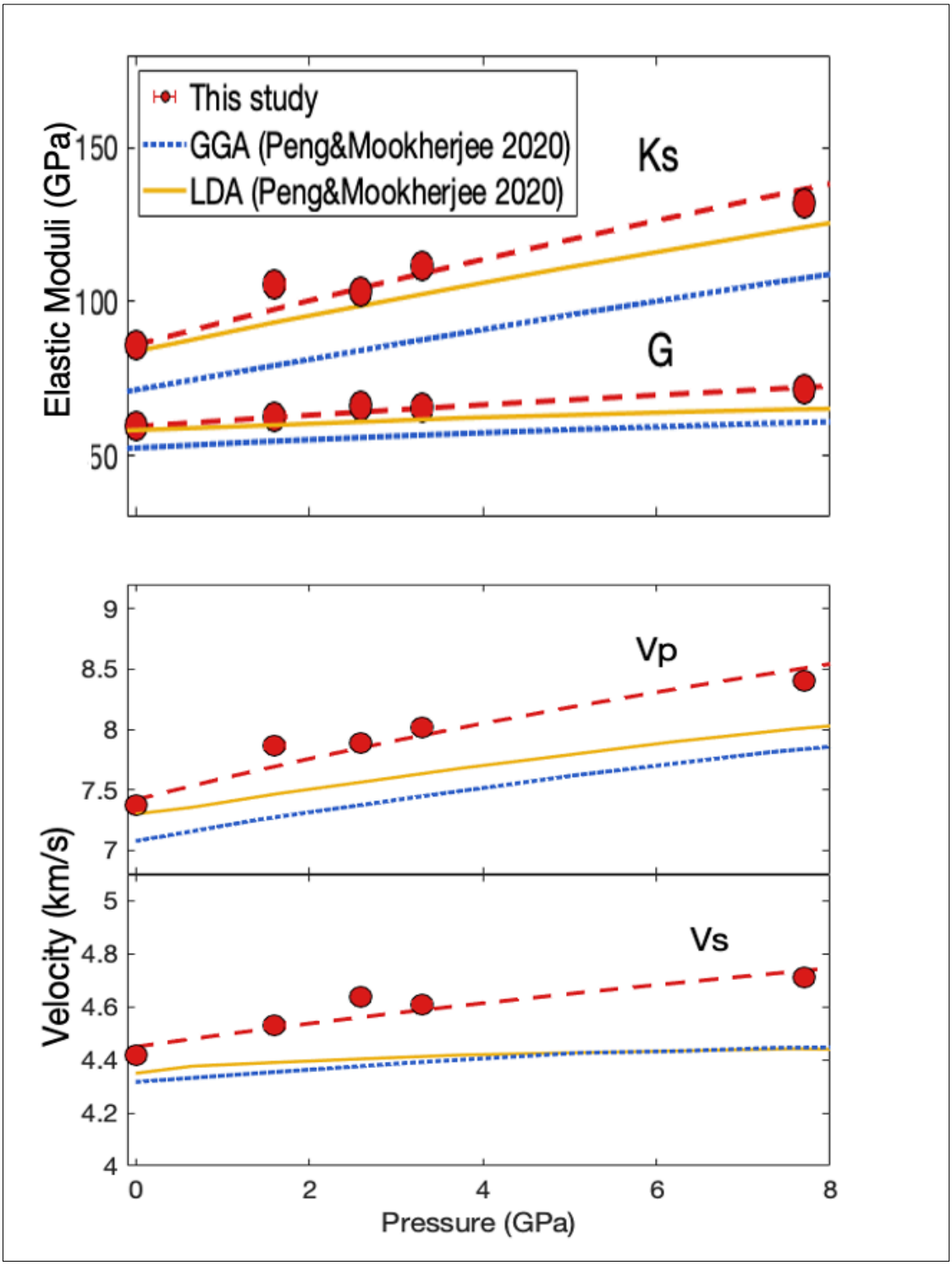

Figure 3.3.1 The Vp, Vs, Ks, and G of single-crystal tremolite at high-P and room-T condition compared with the previous study of Peng and Mookherjee (2020)

b. C_{ij}s at high-pressure condition

The pressure dependance of the C_{ij}s of this study are determined as C_{11}' =5.9±0.002, C_{11}'' =-0.002±0.8, C_{22}' =28.8±1, C_{22}'' =-7.6±0.4, C_{33}' = 24.8±0.8, C_{33}''= -5.4±0.3, C_{44}' =0.56±0.2, C_{44}'' =-0.1±0.01, C_{55}' = 1.05±0.7, C_{55}'' =-0.04±0.1, C_{66}' = 4.6±1.2, C_{66}'' = -0.8±0.4, C_{12}' =5.04±3.1 , C_{12}'' = -0.003±0.04, C_{13}' = 11.3±1.6, C_{13}'' =2.7±0.1, C_{23}' =18.05±0.3, C_{23}'' =-5.4±0.1, C_{15}' =12.3±0.2, C_{15}'' =-3.2±0.09, C_{25}' =1.5±0.9 , C_{25}'' =-0.9±0.11, C_{35}' = 1.8±0.8, C_{35}'' = -0.003±0.04, C_{46}' =1.9 ±0.2, and C_{46}'' =-0.7±0.06.

From the first-principles computational study of Peng and Mookhergjee (2020), all pressure dependance of the principal C_{ij}s (C_{11}, C_{22}, and C_{33}) are greater than 0, indicating the stiffening of tremolite crystal structure upon increasing the pressure. The principal C_{ij}s of this study also shows a similar systematic pattern. The pressure derivatives of C_{22} and C_{33} of Peng and Mookhergjee (2020) are larger than that of the off-diagonal and the shear elastic moduli similar to the C_{22}, and C_{33} of this study. All the unique monoclinic moduli such as C_{25} and C_{35} are not sensitive to pressure. The measured velocities of single-crystal tremolite at 1.6 GPa associated with the velocity model predicted by the C_{ij} model of tremolite are shown on Figure 3.3.2. Some of the pressure derivative from this study are relatively large compare to Peng and Mookherjee (2020), which is likely due to the poorly constrained data at 7.7 ±0.1 GPa. Some of the Vs peaks overlapped with the pressure-transmitting medium at 7.7 ±0.1 GPa. The discrepancies on C_{ij}s' between this study and the computational study may arise due to the velocity constraints of only one orientation in this study and compositional effects. All the best-fit C_{ij}s models are plotted in Figure 3.3.3.

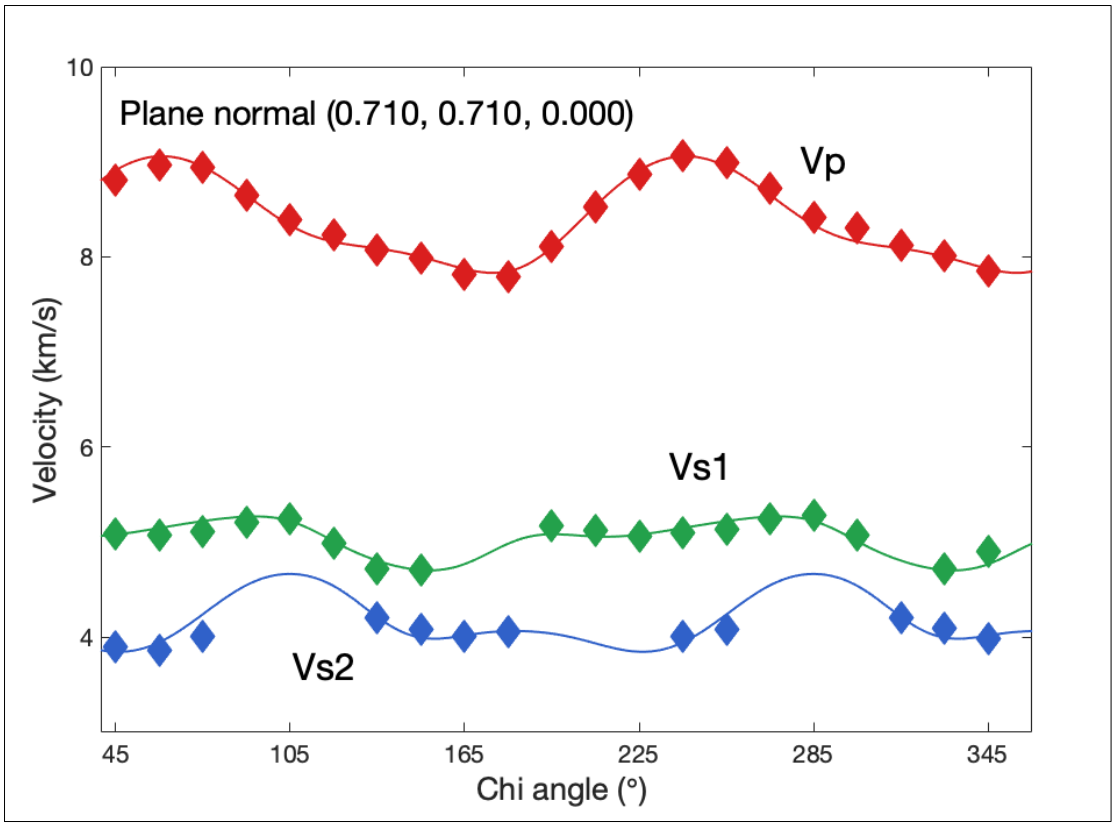

Figure 3.3.2 Measured velocities of the single-crystal tremolite as a function of the chi angles for (0.710, .710, 0.000) orientation at 1.6 GPa. Solid lines are the acoustic velocities calculated from the best-fit single-crystal elasticity model; Closed symbols are the experimentally determined velocities. Errors are within the size of the symbols. The RMS error is 67.14 m/s.

Table 3.4 Single-Crystal and Aggregate Elastic Properties of Omphacite at Different Pressures Determined in This Study

Pressure (GPa)	1 atm	1.6 ±0.12GPa	2.6±0.1GPa	3.3±0.03GPa	7.7±0.01GPa
ρ (cm^3/g)	3.00	3.05	3.08	3.10	3.23
C_{11} (GPa)	117.9±2	114±2	108±2	124±2	163.4±2
C_{22} (GPa)	188±4	239±3	262.7±3	254±3.5	259±3
C_{33} (GPa)	180.9±1.7	224±1.5	230±1	237.4±1.4	257.4±1
C_{44} (GPa)	78.9±2	85±1	85±0.8	84±1	86±0.8
C_{55} (GPa)	63.5±1.5	67±1.4	79±1.5	76.4±1.7	78.4±1.5
C_{66} (GPa)	46.6±2.5	62±1.4	59±1	57.3±1.4	68.7±1
C_{12} (GPa)	57.9±2	60±2	51±1.5	65±1.5	94.3±1
C_{13} (GPa)	55.2±2.9	82±2	68.4±2	74 ±2	92.4 ±1
C_{23} (GPa)	42±2	80±2	90±2	89±2.4	78.4±2
C_{15} (GPa)	-10±2	-5.3±1.6	4.4 ±1.5	6.6±1.7	-5.3±6
C_{25} (GPa)	-4.9±1.5	-10±1.6	-18±1.5	-7.5±1.6	-15.7±1
C_{35} (GPa)	-27.3±1.6	-26±1.2	-28±1.5	-28.5±1	-15.7±1
C_{46} (GPa)	2.3±0.4	1.7± 0.4	5.2±1	5.5±1	1.46 ±1
K^R (GPa)	80±1	98± 1	93±0.8	104±1	129±0.8
G^R(GPa)	56±1	59± 0.5	62±0.5	62±0.6	69±0.5
K^V (GPa)	92±1	113 ±1	113±0.8	119 ±1	134± 0.8
G^V(GPa)	62±1	66± 0.5	71±0.5	69±0.6	74±0.5
K^{VRH} (GPa)	86±7	105±8	103±10	111±8	132±3
G^{VRH}(GPa)	59±4	62± 4	66±4	66±4	71±3
Vp (km/s)	7.4± 0.1	7.8 ± 0.1	7.9 ±0.1	8.0±0.1	8.4 ±0.1
Vs (km/s)	4.4± 0.1	4.5± 0.1	4.6 ±0.1	4.6 ±0.1	4.7±0.1
RMS (m/s)	65.83	67.14	53.32	63.20	56.16

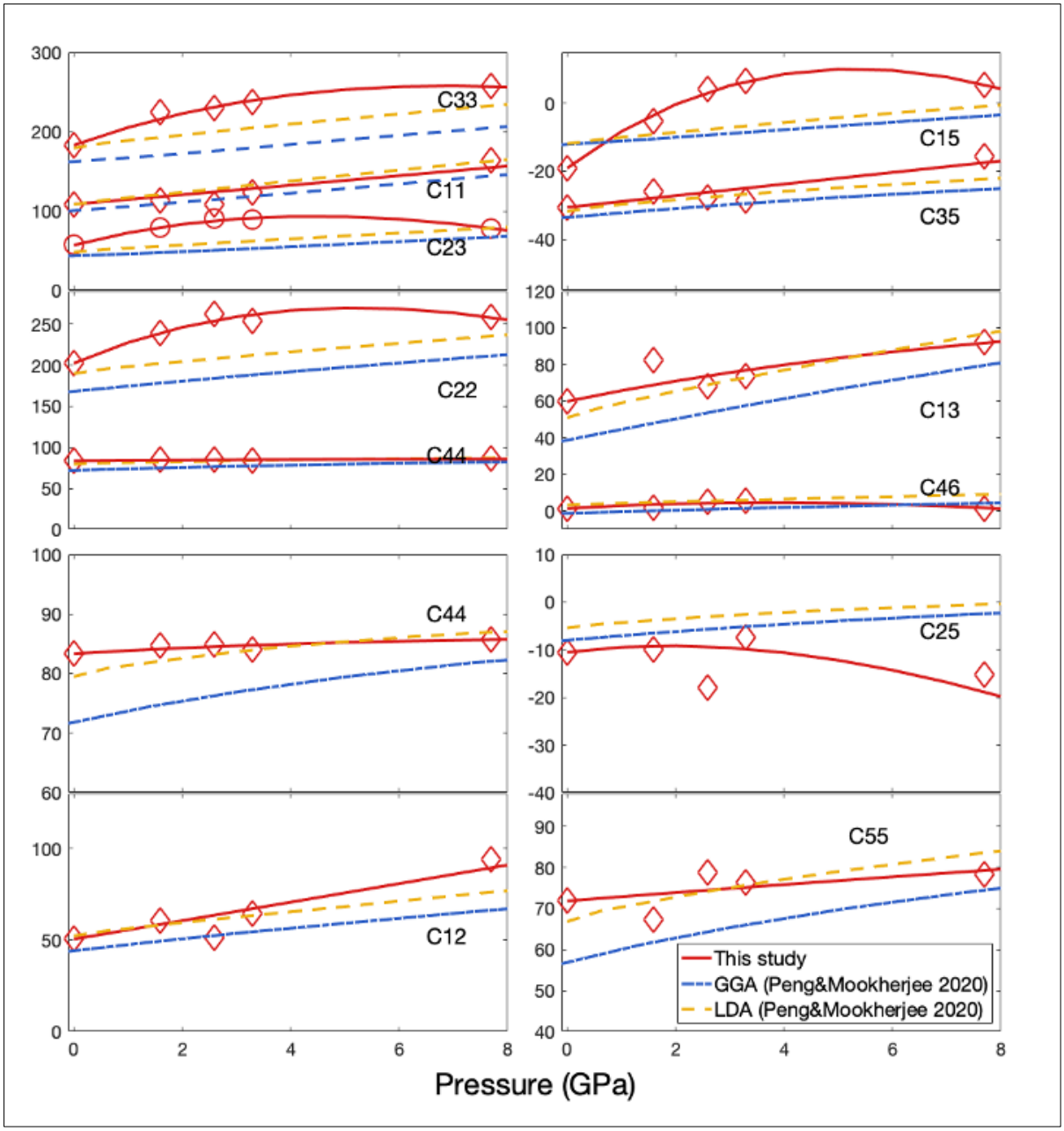

Figure 3.3.3 Single-crystal elastic moduli of tremolite at different pressures in this study and Peng and Mokherjee (2020). The solid red lines represent the best fit finite strain elastic models. The blue line and yellow dotted line are the GGA and LDA approximation, respectively.

c. Anisotropy indices of tremolite and other mantle minerals

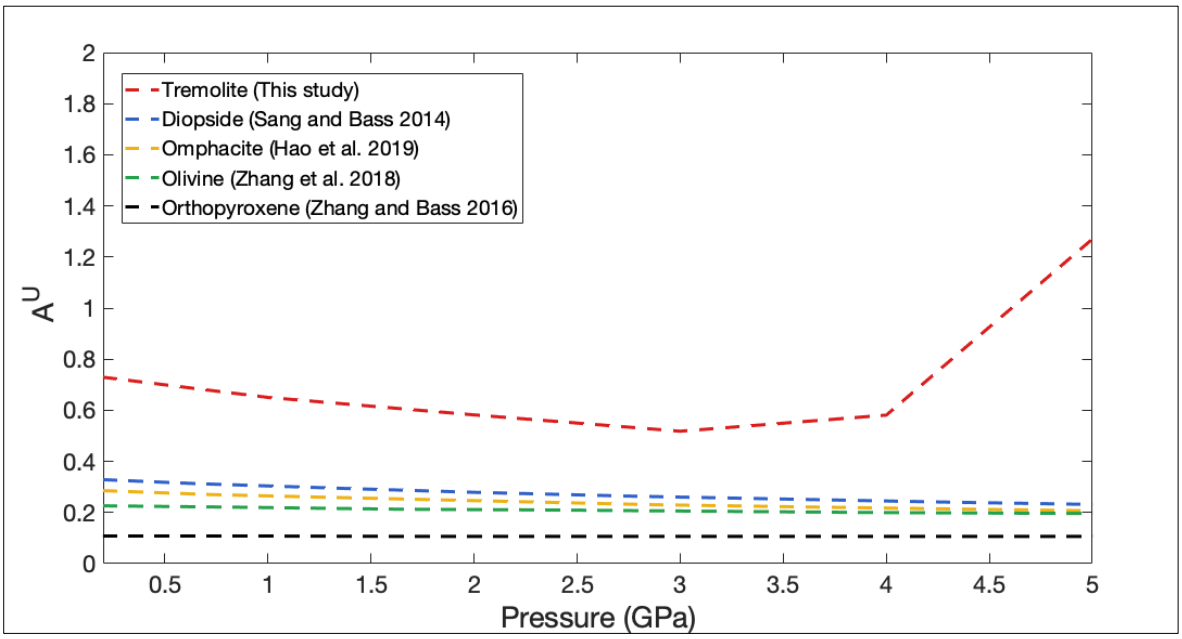

Figure 3.3.4 The anisotropy universal index (A^U) of single-crystal tremolite at 300K from 1 atm to 5 GPa comparing with other major upper mantle minerals in previous studies.

The anisotropy universal index (A^U) of single-crystal are plotted in Figure 3.3.4 along with the A^U of diopside (Sang and Bass 2014), Omphacite (Hao et al. 2019), Olivine (Zhang et al. 2018), and Orthopyroxene (Zhang and Bass 2016). At the ambient condition, the A^U of tremolite is 0.749 and gradually decreases to 0.581 at 4 GPa. Then, the A^U starts to increase in again and rises to >1.0 at 5 GPa. Regarding other anhydrous mantle minerals, the A^U of diopside, omphacite, olivine, and orthopyroxene fall in the range of 0.1 to 0.35 throughout the pressure range of 0-5 GPa. Based on this index, tremolite is more anisotropic than diopside, omphacite, olivine, and orthopyroxene at these given P-T conditions.

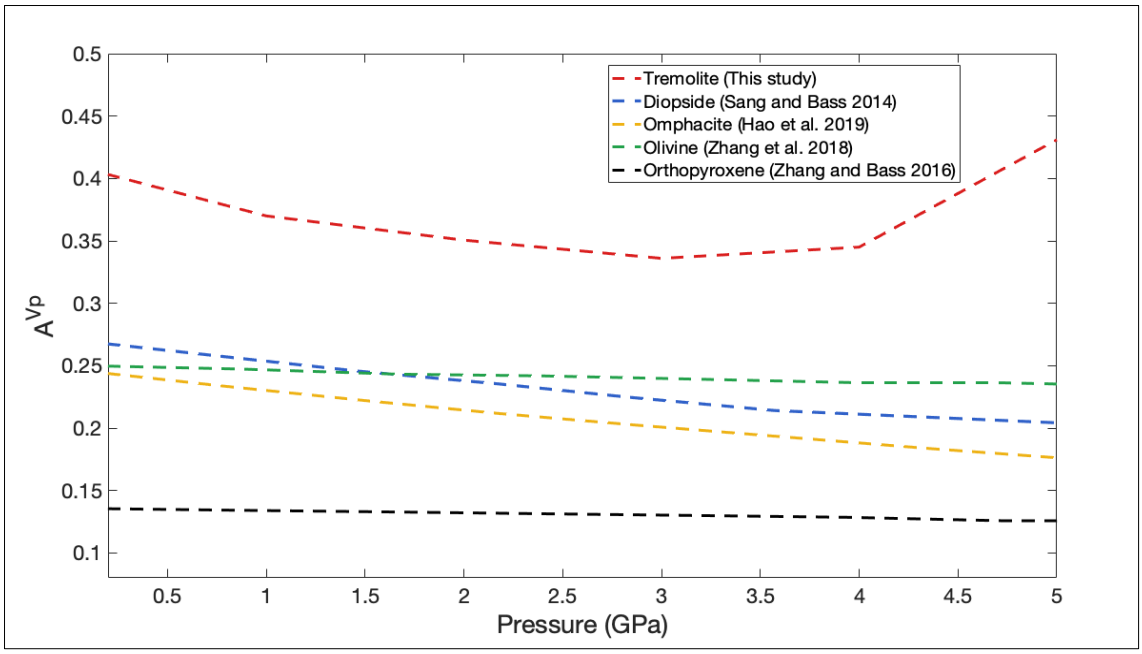

Figure 3.3.5 A^{Vp} of single-crystal tremolite at 300K from single-crystal tremolite at 300K from 1 atm to 5 GPa comparing with other major upper mantle minerals in previous studies.

Throughout the pressure range of 0-10 Gpa, the A^{Vp} of olivine, diopside, omphacite, and orthopyroxene from previous study appear to be gradually decrease with pressure. Most of them have A^{Vp} of approximately 0.25, except for that of orthopyroxene (Zhang and Bass 2016). In comparison to this study, the A^{Vp} of tremolite is 0.412, which is about 1.6 times highr than Avp of olivine, diopside, and omphacite. The A^{Vp} determined in Peng and Mookherjee (2020) is about 0.35 at ambient condition, which is smaller than our result.

At the pressure of 3 GPa, A^{Vp} from Peng and Mookherjee (2020) reduces by 25% to 0.295. Our A^{Vp} decreases to about 0.336, which accounts for 23% reduction of the A^{Vp}. This decrease in A^{Vp} means our data are showing systematic agreement with their results upon increasing the pressure.

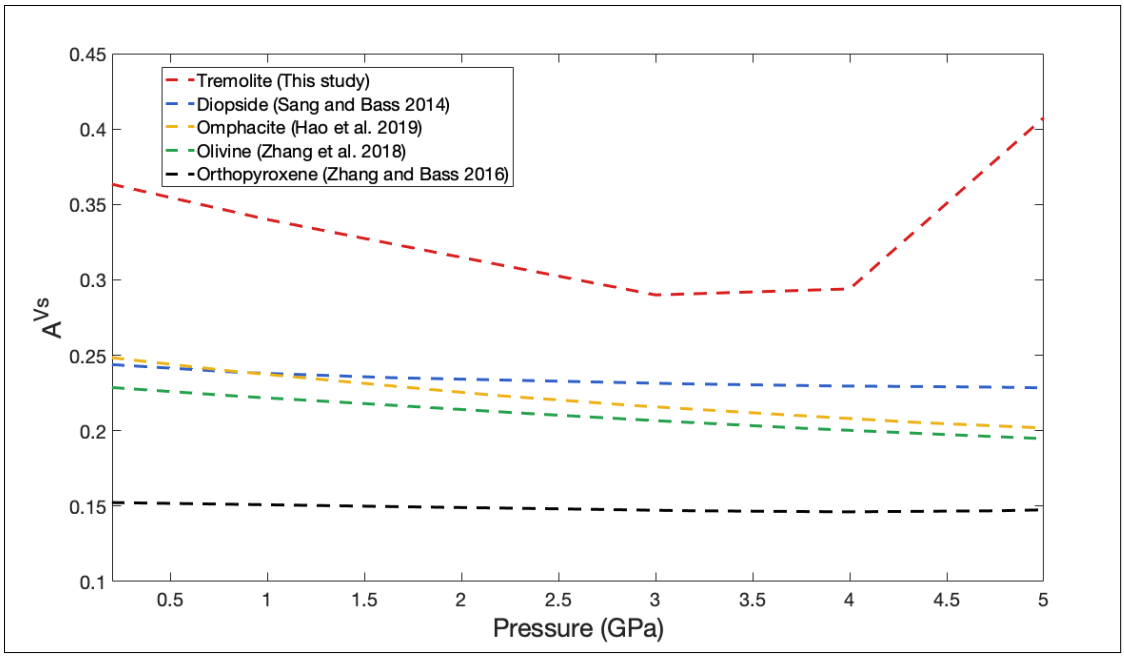

Figure 3.3.6 A^{Vs} of single-crystal tremolite at 300K from single-crystal tremolite at 300K from 1 atm to 5 GPa comparing with other major upper mantle minerals in previous studies

At the ambient condition, the A^{Vs} of tremolite in this study is 0.360, and it gradually decreases with pressure up to 4 GPa as depicted in Figure 3.3.6. For the A^{Vs} of Peng and Mookherjee (2020), their ambient A^{Vs} is about 0.25, which is less than our result. At 3 GPa, the A^{Vs} of Peng and Mookherjee (2020) increases to about 0.3, which is closer to our A^{Vs} of 0.33. Comparing with other major upper mantle minerals, the A^{Vs} of olivine, diopside, and omphacite reside within the range of 0.22-0.25, before gradually decreasing upon increasing the pressure. In summary, the A^{Vs} also suggests that tremolite is more anisotropic than those of other mantle minerals throughout these investigated pressures.

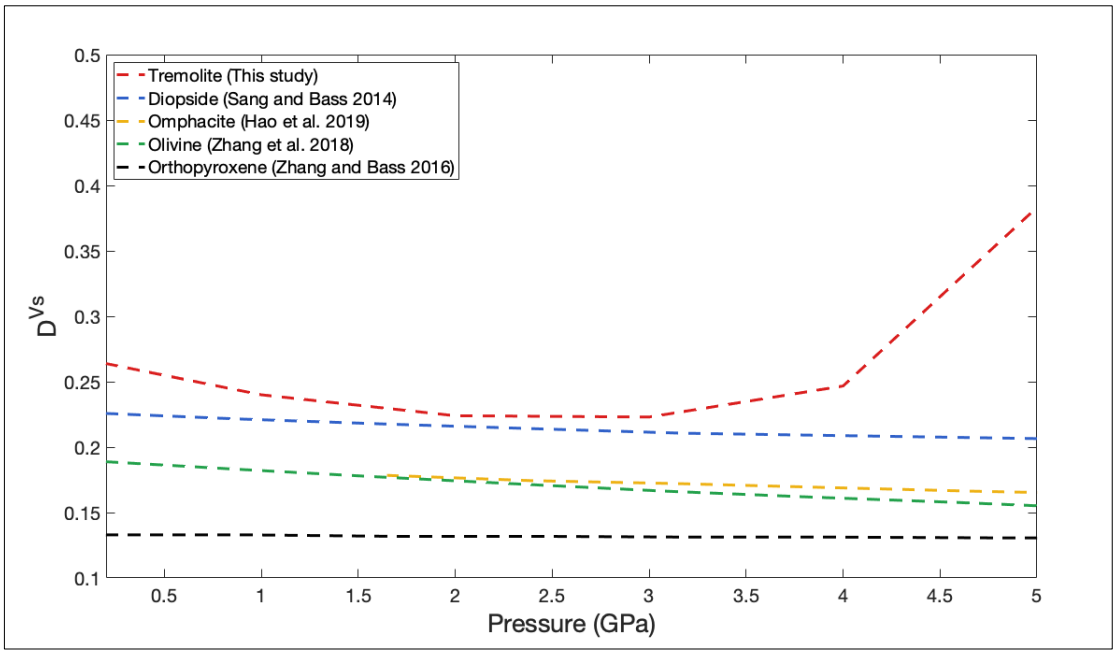

Figure 3.3.7 D^{Vs} of single-crystal tremolite at 300K from single-crystal tremolite at 300K from 1 atm to 5 GPa comparing with other major upper mantle minerals in previous studies

The D^{Vs} depends on the maximum velocity difference of two shear waves that are propagating in the same direction with orthogonal polarization. The D^{Vs} of this study at ambient condition is 0.269, which is also higher than those of olivine, diopside, omphacite, and orthopyroxene from previous study. When the pressure is increased, the D^{Vs} of tremolite gradually decreases until about 4-4.5Gpa, where they start increasing at even higher rate. On the contrary, the D^{Vs} of olivine, diopside, and omphacite all gradually decrease throughout the investigated pressure range.

4. Implications

4.1 Petrological and geochemical evidence of the MLD

To assess the plausibility of the hydrous mineral hypothesis, the compilation of the petrological and geochemical data that verify that these phases are present at the MLD depth is required.

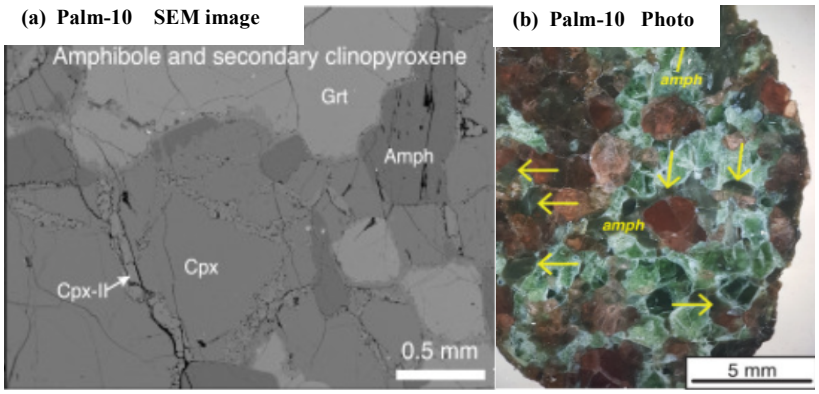

Figure 4.1.1 Metasomatized amphibole-bearing eclogite found under central Kaapvaal craton (Smart et al. 2021) a) metasomatized eclogite under the light microscope showing the crystallization of amphibole b) dark green amphibole grains were indicated by yellow arrows.

The occurrence of hydrous minerals in the cratonic lithosphere may derive from the infiltration of the metasomatic agent that in turns crystallizing an assemblage of secondary minerals. Generally, the abundance of amphibole and phlogopite is controlled by the bulk alkali content, relative abundance of major cations, water, and temperature (Saha et al. 2021). According to the petrological and geochemical study on metasomatized eclogite xenoliths from the Kaapvaal craton by Smart et al. (2021), the occurrence of altered eclogites that are rich in amphibole, phologopite, and magnesite are comfirmed as depicted in Figure 4.1.1. Their analysis suggested that these samples used to reside at the depth of 85 kilometers,

corresponding to the MLD layer detected under the Central Kaapvaal craton (e.g. Sodoudi et al. 2013). The Pb isotope from their study indicated potassic-rich melts as a metasomatic agent, and their results point to the calcic to sodic-calcic amphiboles to be parts of these metasomatized and low-velocity layer at the MLD depth (Smart et al. 2021)

Rader et al. (2015) also compiled the xenolith data from the PetDB database with the criteria that those xenoliths were found within the continental area, contained geochemical information, and came from the MLD depth. From their results, 44 out of 174 xenoliths consisted of amphibole or phlogopite from the depth corresponding to the pressure of 0.2-6.5 GPa. They had postulated the hypothesis that melts were derived from a deeper interior and undergone crystallization once it reach the stability field of these hydrous phases (~3 GPa.). The solidification of these melts turned into a compact layer and resulted in a gradient of negative velocity phases (e.g. Rader et al 2015; Sparks and Parmentier 1991). Another study from Wang and Kusky et al. (2019) also reported the occurrence of a amphibole/ phlogopite/chlorite/carbonatite -bearing layer within the Karelian craton.

4.2 Proposals of the abundance of amphibole at the MLD depth

With the possibility of amphibole contributing to the negative velocity gradients of the MLD, several publications have quantitatively examined the appropriate abundance of amphiboles that can lead to the observed velocity drops at MLD. Selway et al. (2015) had used the mineral physics model based on Hacker and Abers (2014) and seismic receiver function observations to simulate the condition for the MLD. They reported that 25% of amphibole along with 1% of phlogopite were likely to cause a velocity reduction at the MLD depth by 4.4% (Selway et al. 2015). Peng and Mookherjee (2020) also utilized their computational

results and postulated that 25% of amphibole were likely to cause a velocity reduction by 1.9%. Saha et al (2018) compiled experimental phase equilibrium data on various hydrous peridotite compositions, and found that with less than 1% CaO in the cratonic mantle lithosphere, the abundance of amphibole is 10-15% at the relevant P-T conditions. They suggested that 10-15% of amphibole combining with 5% phlogopite were needed to reproduce the velocity reductions of MLD. Both Selway et al. (2015) and Saha et al. (2018) found that the velocity reduction caused by the existence of reasonable amount of amphibole and phlogopite could not cover the entire range of Vp and Vs drop observed over the globe. Other mechanisms are needed to contribute to the MLD for the regions where large velocity reductions have been observed (e.g. grain boundary sliding, fine-scale heterogeneity, change in azimuthal anisotropy etc). However, these aforementioned previous modelling studies were based on either the ambient elasticity data or computationally calculated elasticity data of relevant hydrous phases. Future modelling based on the new results from this study may provide a more complete idea on how the hydrous phases would behave under high-P condition.

4.3 Velocity comparison and anisotropy

To further explore the role of tremolite amphibole in contributing to the high anisotropy and low velocity at MLD depth, comparison with the velocity and anisotropy of common mantle rocks are needed.

Xu et al. (2008) calculated the Vp and Vs of mantle rocks with different compositions in chemical equilibrium and mechanical mixtures along a 1600 K mantle adiabat in the Earth's interior. At the MLD depth (~100 km), the Vp and Vs of harzburgite are 7.8 and 4.4 km/s, respectively. At the same P-T condition, the Vp and Vs of basalt are 7.8 and 4.7 km/s,

respectively. In comparison, the Vp and Vs of tremolite determined at 3 GPa 300 K in this study are 8.0 and 4.6 km/s, which are comparable to the velocities of harzburgite at similar pressure but much higher temperature at 1700 K (Katsura et al. 2010). Since velocities decrease significantly with temperature, we expect the velocity of tremolite at high P-T conditions to be significantly slower than these mantle rock aggregates under MLD conditions. However, the data presented in this study relied on the velocity measurements only within the (110) plane. Due to the overlap between the Brillouin peak of Vs of the tremolite crystal and the pressure-transmitting media, many inverted high-pressure elastic properties may not be reliable. Future experiments on the single-crystal tremolite for different orientations at simultaneously high pressure-temperature conditions are needed.

Yuan and Romanowicz (2010) reported the change in azimuthal anisotropy underneath craton in North America. They suggested that a petrological boundary (i.e. MLD) separated the cold and depleted Archean craton from the less-depleted hotter layer. The anisotropy change can be caused by the different textures formed in those two layers. If the MLD is caused by the existence of amphibole dominated rock assembly, then the anisotropy resulted from the LPO of amphibole would surely be different from the anisotropy in the anhydrous mantle rock aggregate. Future anisotropy modeling based on the single-crystal elasticity measured in this study and previous deformation experiments (e.g. Jung and Ko 2015) is required for better quantification of the MLD anisotropy.

The universal cause of the MLD remains debatable due to the wide range of the observed depth thus the P-T conditions near MLD and the complicated lithologies in the cratonic lithosphere. For example, the crystallized hydrous mineral layer which could contain phlogopite or amphibole may not be responsible for the MLD observed at more than 150-km

depth due to the stability of these hydrous phases. The investigation on the elasticity of tremolite at simultaneously high P-T conditions are needed to provide mineral physicists and geophysicist more constraints to the seismic velocities and anisotropy of amphiboles at MLD conditions in nature. Therefore, the origin of the MLD has remained an open question and is crucial for understanding the geophysical observations and geochemical evolution of the lithospheric mantle under stable cratons.

5.Conclusion

Tremolite is a Ca-endmember amphibole and belongs to the double-chain silicate group with a monoclinic C2/m structure. We measured its high-pressure single-crystal elastic properties for the first-time using Brillouin spectroscopy, which are determined as C_{110} =118±2, C_{220}=188±4, C_{330}=181±2, C_{440}=79±2, C_{550}=64±2, C_{660}=47±3, C_{120}=58±2, C_{130}=55±3, C_{230}=42±2, C_{150}=-10±2, C_{250}=-5±2, C_{350}=-27±2, C_{460}=2.3±0.4, Ks_0= 86±6 GPa, G_0= 59±4 GPa, Ks'=7.5±3, G'=1.9±1, C_{11}' =5.9±0.002, C_{11}'' =-0.002±0.8, C_{22}' =28.8±1, C_{22}'' =-7.6±0.4, C_{33}' = 24.8±0.8, C_{33}''= -5.4±0.3, C_{44}' =0.56±0.2, C_{44}'' =-0.1±0.01, C_{55}' = 1.05±0.7, C_{55}'' =-0.04±0.1, C_{66}' = 4.6±1.2, C_{66}'' = -0.8±0.4, C_{12}' =5.04±3.1 , C_{12}'' = -0.003±0.04, C_{13}' = 11.3±1.6, C_{13}'' =2.7±0.1, C_{23}' =18.05±0.3, C_{23}'' =-5.4±0.1, C_{15}' =12.3±0.2, C_{15}'' =-3.2±0.09, C_{25}' =1.5±0.9 , C_{25}'' =-0.9±0.11, C_{35}' = 1.8±0.8, C_{35}'' = -0.003±0.04, C_{46}' =1.9 ±0.2, and C_{46}'' =-0.7±0.06. Our Ks_0 and G_0 are in general agreement with the *first-principles* study of thermoelastic properties of tremolite from Peng and Mookherjee (2020). However, our inverted high-pressure elastic properties are different from Peng and Mookherjee (2020). The discrepancies may arise from the compositional effects and/or the availability of velocity measurements along more crystallographic directions. Comparing the velocities with other major upper mantle minerals such as olivine, clinopyroxene and orthopyroxene, tremolite has

generally slower Vp and Vs. The anisotropy indices of tremolite in this study suggested that tremolite is more anisotropic than other major upper mantle minerals throughout the investigated pressure range. The limited data of tremolite here seems in support of the possible contribution of amphiboles to the seismic observations near MLD. However, this study mainly relied on the velocities measured within the (110) plane. Future studies of elasticity of amphibole at high pressure-temperature conditions along more crystallographic directions are required to evaluate its role in generating the MLD under cratons.

Appendix

Supplementary Materials

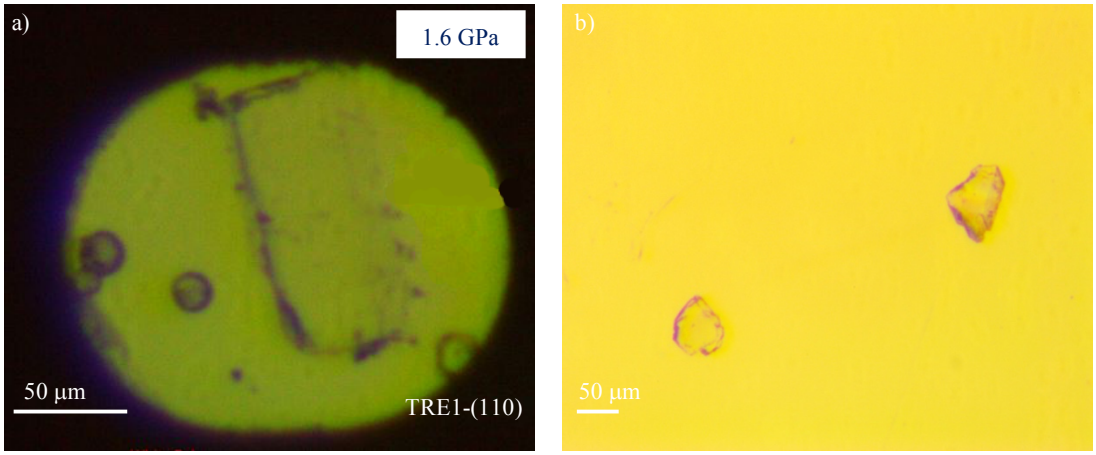

Figure S1: a) Photographs of the sample chambers inside the DAC assembly of single-crystal Tremolite (110) TRE1 at room temperature and 1.6 GPa. These cells were loaded with methanol-ethanol (4:1) pressure medium and rubies for pressure calibration. The gasket hold decreased in diameter upon increasing the pressure. b) Two tremolite crystals were placed in the DAC for the X-ray diffraction experiments.

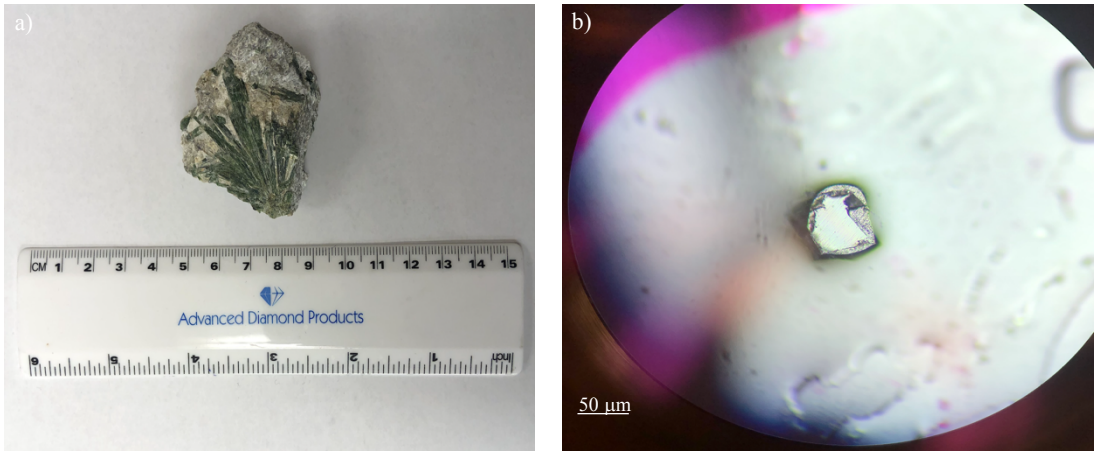

Figure S2: a) A hand specimen of TRE1 sample $(Na_{0.09}\ (Ca_{1.98}\ Na_{0.02})(Mg_{4.735}Mn_{0.01}\ Al_{0.24})(Si_{7.72}Al_{0.28})O_{22}(OH)_2)$ before the sample preparation processes. b) A single-crystal tremolite under the light microscope during the polishing process. A smooth and clean crystal face would result in the successful and accurate velocity measurement.

Table S1. Chemical analysis of Tremolite amphiboles for this project and previous elasticity study

Element Formulae	TRE1	Ca-Na Amphibole (Brown and Abramson 2016)
K	0.00	0.009
Ca	1.98	1.741
Na	0.11	0.146
Si	7.72	7.718
Al	0.52	0.395
F	0.00	0.035
OH	2.00	1.992
Ti	0.00	0.002
Cr	0.00	0.035
Mn	0.01	0.040
Mg	4.735	4.072
Fe	0.00	0.738

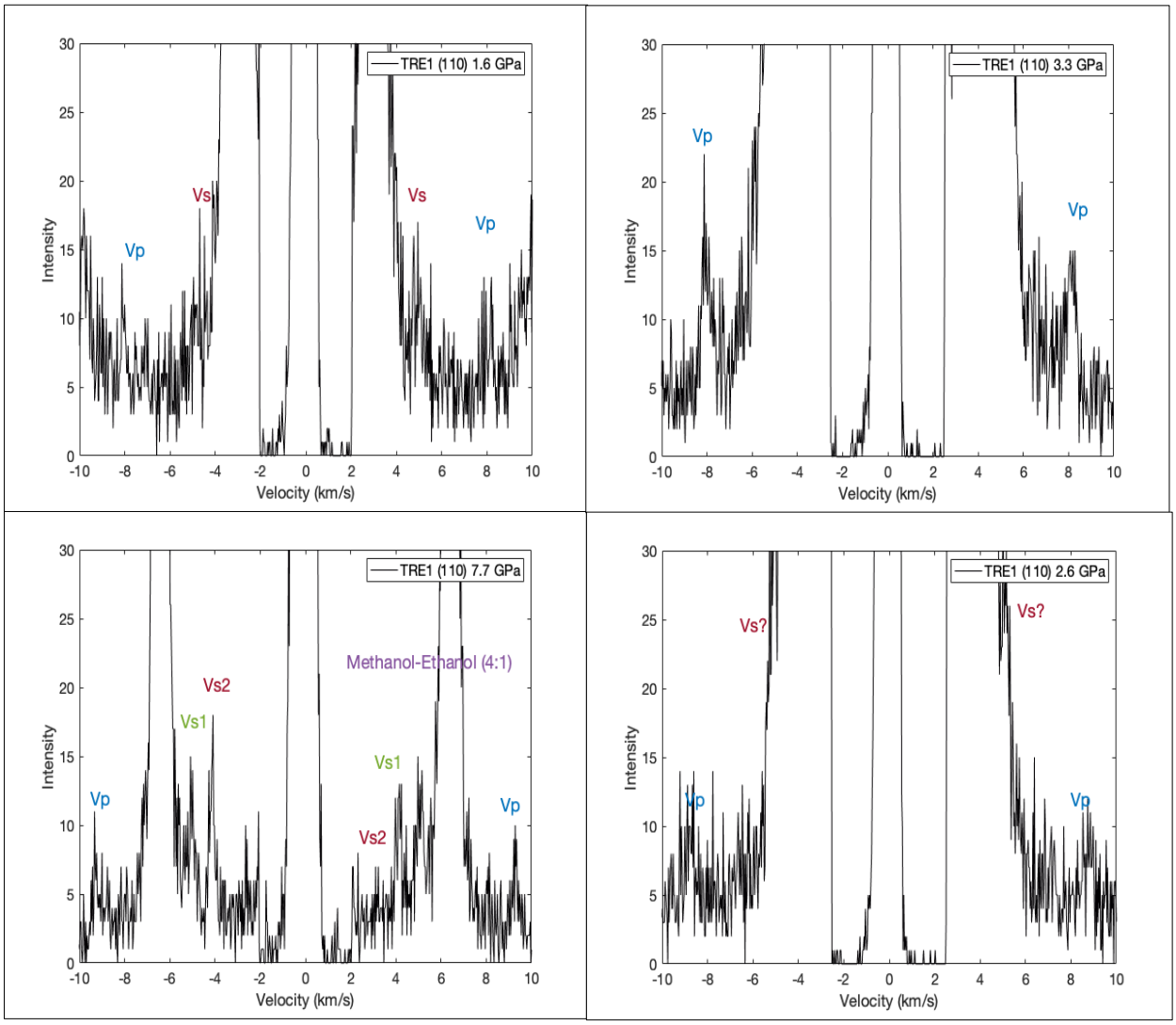

Figure S3: Brillouin spectra of TRE1 under different pressure conditions. Two prominent peaks of methanol-ethanol-water mixture can be observed at each pressure. The velocity peaks of TRE1 become more distinct and sharper as the pressure increases since the refractive index of the methanol-ethanol-water mixture increases with pressure.

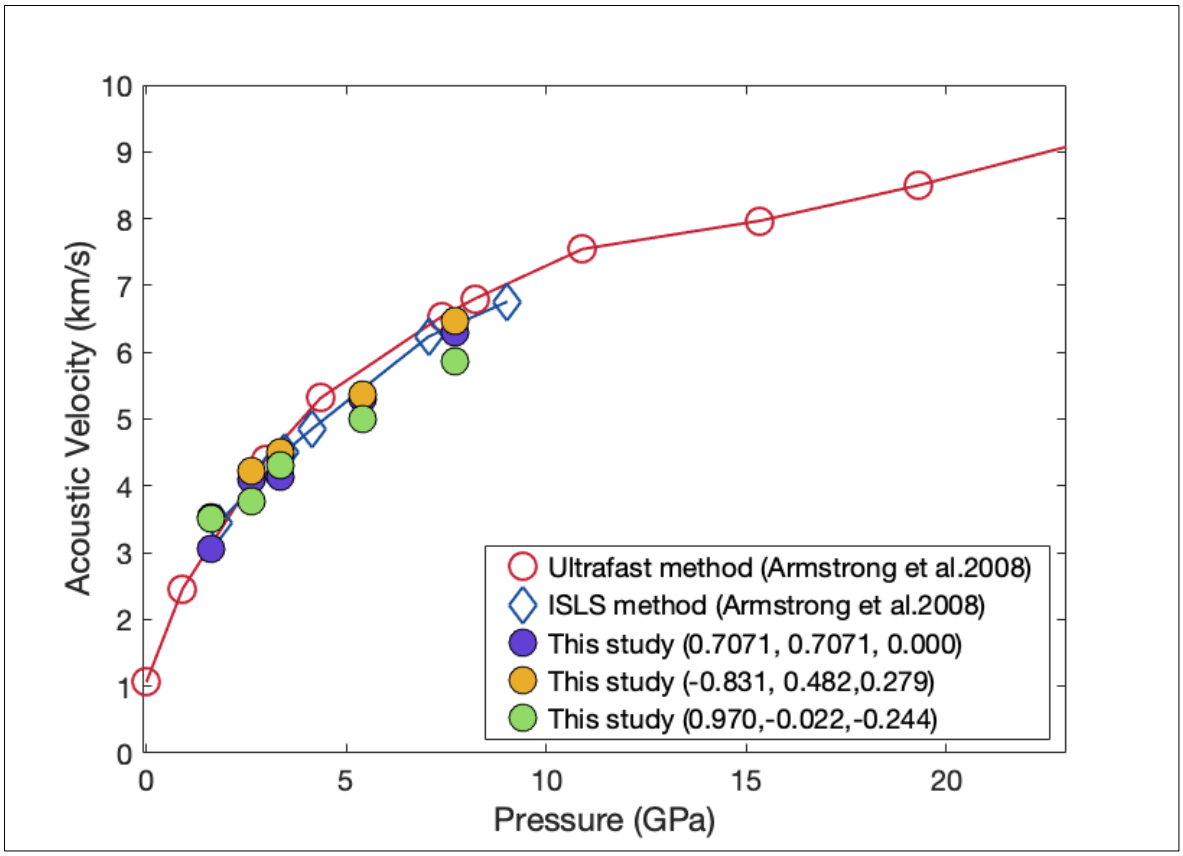

Figure S4: Acoustic velocity measurements of the 4:1 methanol-ethanol mixture as a pressure medium in the Brillouin experiments are plotted in comparison to previous study using different methods.

References

Abramson E.H., Brown J.M., Slutsky L.J. 1999. Application of impulsive stimulated scattering in the Earth and planetary sciences. *Annu. Rev. Phys.Chem,* ***50*****,** 279-313

Abt D., Fisher K.M., French S.W., Ford H.A., Yuan H., Romanowicz B. 2010. North American lithospheric discontinuity structure imaged by Ps and Sp receiver functions. *Journal of Geophysical Research,* ***115***

Anderson, J.L. and Smith, D.R. (1995) The effects of temperature and *f* on the Al-in-hornblende barometer. *American Mineralogist*, ***80***, 549– O2 559.

Bailey D.K. 1082. Mantle metasomatism-continuing chemical change within the Earth. *Nature,* ***296***, 525-530

Bascou J., Barruol G. Vauchez A., Mainprice D., Egydio-Silva M. 2001. EBSD-measured lattice-preferred orientations and seismic properties of eclogites. *Tectonophysics,* ***342****,* 61-80

Bass J.D., Parise J.B. 2008. Deep earth and recent developments in mineral physics. *Elements,* ***4***(3), 157-163

Bass J.D., Sinogeikin S., Li B. 2008. Elastic properties of minerals: a key for understanding the composition and temperature of earth interiors. *Elements,* ***4,*** 165-170

Bina C.R., Helffrich G.R. 1992. Calculation of elastic properties from thermodynamic equation of states principles. *Annu. Re* (Abramson E.H., 1999) *Earth Planet Sci,* ***20****,* 527-552

Bina, C.R.; Stein, S.; Marton, F.C.; Van Ark, E.M. Implications of slab mineralogy for subduction dynamics. *Phys. Earth Planet. Inter*. 2001, 127, 51–66

Bina, C.R.; Kawakatsu, H. Buoyancy, bending, and seismic visibility in deep slab stagnation. *Phys. Earth Planet. Inter.* 2010, 183, 330–340

Brown J.M., Abramson E.H. 2016. Elasticity of calcium and calcium-sodium amphiboles. *Physics of the Earth and Planetary Interiors,* ***261****,* 161-171

Cairney J.M., Munroe P.R., Schneibel J.H. 2000. Examination of fracture surface using focused ion beam milling. *Scripta Mater****, 42,*** 473-478

Carlson, R.L.; Miller, D.J. Mantle wedge water contents estimated from seismic velocities in partially serpentinized peridotites. *Geophys. Res. Lett.* 2003, ***30***, 1250.

Cameron M., Sueno S., Prewitt T., Papike J. 1973. High-temperature crystal chemistry of acmite, diopside, hedenbergite, jadeite, spodumene, and ureyite. *Amer. Mineral.* ***58***, 594-618

Cameron M., Sueno S., Prewitt T., Papike J. 1973. The high-temperature crystal chemistry of tremolite.*Amer. Mineral.* ***58***, 649-652

Carlson R.W., Pearson D.G., James D.E., 2005. Physical, chemical, and chronological characteristics of the continental mantle. *Rev. Geophys.* ***43***, 24

Ceperley D.M., Adler B.J. 1980. Ground state of electron gas by a stochastic method. *Physical Review Letters,* ***45***, 566-569

Chernosky J.V., Berman R.G., Jenkins D.M. 1998. The stability of tremolite; new experimental data and a thermodynamic assessment. *American Mineralogist,* ***83***(7-8), 726-739

Christoffel E.B. 1877. Über die Fortpflanzung von Stössen durch elastische feste Körper. *Annali di Matematica Pura ed Applicata,* ***8***(2), 193-243

Comidi P., Mellini M., Ungaretti L., Zanazzi PF. 1991. Compressibility and high-pressure refinement of tremolite, pargasite, and glaucophane. *Eur J Mineral*. 3:485-499

Dasgupta R. 2013, Ingassing, storage, and outgassing of terrestrial carbon through geologic time. *Rev. Mineral. Geochem,* ***75***, 183-229

Dasgupta R., Hirschmann M.M. 2010. The deep carbon cycle and melting in the Earth's interior. *Earth Planet. Sci. Lett,* ***184***, 339-351

DeBari, S.M., and Coleman, R.G., 1989, Examination of the deep levels of an island arc: Evidence from the Tonsina ultramafic-mafic assemblage, Tonsina, Alaska: *Journal of Geophysical Research*, ***94***, p. 4373–4391.

Deer W.A., Howie R.A., Zussman J. 1997. *Rock-forming minerals: double-chain silicates,* ***2B*****,** 136-141

Delpech, G., Gregoire, M., O'reilly, S., Cottin, J., Moine, B., Michon, G., & Giret, A. 2004. Feldspar from carbonate-rich silicate metasomatism in the shallow oceanic mantle under Kerguelen Islands (South Indian Ocean). *Lithos,* ***75***, 209-237.

Ernst, W., & Liu, J. (1998). Experimental phase-equilibrium study of Al- and Ti-contents of calcic amphibole in MORB—A semiquantitative thermobarometer. *American Mineralogist,* ***83***, 952 - 969.

Ford H.A., Long M.D., Wirth E.A. 2016. Mid lithospheric discontinuities and complex anisotropic layering in the mantle lithosphere beneath the Wyoming and Superior provinces. *J. Geophysics.Res,* ***121***(9), 6675-6679

Frost D.J. 2006. The stability of hydrous mineral phases. *Reviews in Mineralogy and Geochemistry,* ***62****,243-271*

Fumagalli P., Zanchetta S., Poli S. 2009. Alkali in phlogopite and amphibole and their effects on phase relations in metasomatized peridotites: a high-pressure study. *Contrib Miner Petrol* ***158****,* 723-737

Gilbert C.M., Helz R.T., Popp R.K., Spear F.S. 1982. Experimental studies of amphibole stability. *Reviews in Mineralogy,* ***9B****,* 245-258

Green, T., Adam, J., & Siel, S. (1992). Trace element partitioning between silicate minerals and carbonatite at 25 kbar and application to mantle metasomatism. *Mineralogy and Petrology, **46***, 179-184.

Green D.H., Hibberson W.O., Kovács L., Rosenthal A. 2010. Water and its influence on the lithosphere-asthenosphere boundary. *Nature, **467***, 448-451

Green D.H., Hibberson W.O., Rosenthal A., Kovács I., Yaxley G.M., Faloon T.J. Brink F. 2014. Experimental study of influence of water on melting and phase assemblages in the upper mantle. *J Petrol, **55***, 2067-2096.

Grove T.L., Chatterjee N., Parman S.W. Médard E. 2006. The influence of H_2O on mantle wedge melting. *Earth Planet Sci Lett, **19***, 37-53

Hacker B.R., Abers G.A., Peacock S.M. 2003. Subduction factory 1. Theoretical mineralogy, densities, seismic wave speeds, and H_2O contents. *J. Geophys. Res., Solid Earth 108*.

Hao M., Zhang J.S., Pierotti C.E., Ren Z., Zhang D. 2019. High-pressure single crystal elasticity and and thermal equation of state of omphacite and their implications for the seismic properties of eclogite in the earth's interior. *Journal of Geophysics Research: Solid Earth, **124***, 2368-2377

Hansen S.M., Dueker K., Schmandt B. 2015. Thermal classification of lithospheric discontinuities beneath USArray. *Earth Planet. Sci. Lett. **431***, 36-47

Hazen R.M., Downs R.T. 2000. High-temperature and high-pressure crystal chemistry. *Reviews in Mineralogy and Chemistry*, **41**, 465-468.

Hawthorne, F.C. (1981) Crystal chemistry of the amphiboles. *Mineralogical Society of America Reviews in Mineralogy*, **9A,** 1–102.

Hawthorne F.C., Oberti R. 2007. Amphiboles: crystal chemistry. *Reviews in Mineralogy and Geochemistry, **67,*** 1-54

Hemley R.J. 1998. Ultrahigh-pressure mineralogy: physics and chemistry of the Earth's deep interior. *Reviews in Mineralogy, **37***,27

Hielscher R., Schaeben H. 2008. A novel pole figure inversion method: specification of the MTEX algorithm. *Journal of Applied Crystallography, **41**(6),* 1024-1037

Hill R. 1952. The elastic behavior of crystalline aggregates. *Philos. Trans. R. Soc. London, Ser. A, **65,*** 349-354.

Hill, R., 1963. Elastic properties of reinforced solids: some theoretical principles. *Journal of the Mechanics and Physics of Solids, **11***(5), 357-372.

Hirschmann M.M. 2006. Water, melting, and the deep earth H_2O cycle. *Annu. Rev. Earth Planet. Sci, **34***,629-593

Hopper E., Fischer K.M. 2015. The meaning of midlithospheric discontinuities: a case study in the northern US craton. *Geochem. Geophys. Geosyst.* ***16***(12), 4057-4083.

Isaak D.G., Ohno I., Lee P.C. 2006. The elastic constants of monoclinic single-crystal chrome-diopside to 1300 K. *Phys. Chem. Mineral,* ***32,*** 691-699.

Jackson J.M., Sinogeikin S.V., Bass J.D. 2007. Sound velocities and single-crystal of orthoenstatite to 1073 K at ambient pressure. *Physics of the Earth and Planetary Interiors,* ***161,*** 1-12

J. BARCLAY, I. S. E. CARMICHAEL, A Hornblende Basalt from Western Mexico: Water-saturated Phase Relations Constrain a Pressure–Temperature Window of Eruptibility, *Journal of Petrology*, Volume 45, Issue 3, March 2004, Pages 485-506

Jon Davidson, Simon Turner, Heather Handley, Colin Macpherson, Anthony Dosseto; Amphibole "sponge" in arc crust?. *Geology* 2007;; 35 (9): 787–790.

Johnson K.E., Davis A.M., Bryndzia L.T. 1996. Contrasting styles of hydrous metasomatism in the upper mantle: An ion microprobe investigation. *Geochimica et Cosmochimica Acta,* ***60***(8), 1367-1385

Jordan T.H. 1988. Structure and the formation of the continental tectosphere. *J.Petrol,* ***29***, 11-37

Ko, B. and H. Jung. "Crystal preferred orientation of an amphibole experimentally deformed by simple shear." *Nature Communications* 6 (2015): n. pag.

Karato S.-I., 2012. On the origin of the asthenosphere. *Earth Planet. Sci. Lett.* ***321***, 95-103

Katsura, T. et al. "Adiabatic temperature profile in the mantle." *Physics of the Earth and Planetary Interiors* 183 (2010): 212-218.

Kim J. Jung H. 2019. New crystal preferred orientation of amphibole experimentally found in simple shear. *Geophysics Research Letters,* ***46,*** 12,996-13,003

Kirby, S.H.; Stein, S.; Okal, E.A.; Rubie, D.C. Metastable mantle phase transformations and deep earthquakes in subducting oceanic lithosphere. *Rev. Geophys*. ***1996***, 34, 261–306.

Ko B. Jung H. 2015. Crystal preferred orientation of an amphibole experimentally deformed by simple shear. *Nature Communication*, 6:6586

Kovács I., Lenkey L., Green D.H., Fancsik T., Falus G., Kiss J., Orosz L., Angyal J., Vikor Z. 2017. The role of pargasitic amphibole in the formation of major geophysical discontinuities in the shallowupper mantle. *Acta. Geod. Geophys.,* ***52***, 183-204

Kong M., Vogt Th., Lee Y. 2018. High-pressure synchrotron X-ray diffraction of tremolite and and various fluids. *Current Applied Physics,* ***18***(11), 1218-1224.

Kube C.M. 2016. Elastic anisotropy of crystals. *AIP ADVANCES,* ***6,*** 095209

Kumar P., Kind R.,Yuan X., Mechie J. 2012. USArray receiver function images of the lithosphere-asthenosphere boundary. Seismological Research Letters, 83(3), 486-491

Ling Chen. 2009. Lithospheric structure variations between the eastern and central North China craton from s- and p-receiver function migration. *Physics of the Earth and Planetary Interiors **173***, 216-227

Liu L., Gao S.S. 2018. Lithospheric layering beneath the contiguous United States constrained by s-to-p receiver function. *Earth and Planetary Science Letter, **495***, 79-85

Lundqvist S., March N.H. 1987. Theory of the inhomogeneous electron gas. Plenum Press, New York

Mainprice D. 1990. An effiecient FORTRAN program to calculate seismic anisotropy from the lattice preferred orientation of minerals. *Computational Geoscience, **16***, 385-393

Mainprice D. 2015. Seismic anisotropy of the deep earth from a mineral and rock physics perspective. *Treatise on Geophysics*, vol.2, pp 487-538

Mandler B.E., Grove T.L. 2016. Controls on the stability and composition of amphibole in the Earth's mantle. *Contrib Miner Petrol **171**,* 68

Mao H.K., Hemley. R.J. 1998. New windows on the Earth's deep interior. *Reviews in Mineralogy, **37***, 27

Mao, Z., Li, X. Effect of hydration on the elasticity of mantle minerals and its geophysical implications. *Sci. China Earth Sci.* **59,** 873–888 (2016). https://doi.org/10.1007/s11430-016-5277-9

McInnes B I A, Gregoire M, Binns R A, Herzig P M, Hannington M D. 2001. Hydrous metasomatism of oceanic sub-arc mantle, Lihir, Papua New Guinea: Petrology and geochemistry of fluid metasomatised mantle wedge xenoliths. *Earth Planet Sci Lett, **188***: 169–183

Mengel K., Green D.H. 1989. Stability of amphibole and phlogopite in metasomatized peridotite under water-saturated and water-under-saturated conditions. In: Ross J (ed) Kimberlites and related rocks: their composition, occurrence, origin and emplacement. 4th international kimberlite conference in Perth, 1986. Vol 1, Blackwell Scientific Publications for the Geological Society of Australia, pp 571-581

Menzies M.A., Rogers N., Tindle A. Hawkesworth C.J. 1987. Metasonatic enrichment processes in lithospheric peridotites, an effect of astenosphric interaction. *In*: Mantle Metasomatism. Menzies M.A., Hawkesworth C.J. (eds) *Academic Press*, 313-361

Miletich R., Allan R.D., Kuhs F. 2000. High-pressure single crystal techniques. *Reviews in Mineralogy and Chemistry*, **41**, 465-468.

Moody, J.B., Meyer, D., and Jenkins, J.E. (1983) Experimental characterization of the greenschist/amphibolite boundary in mafic systems. *American Journal of Science, **283***, 48–92

Musgrave M.J.P. 1970. Crystal acoustic: introduction to the study of elastic waves and vibrations in crystals. Holden-Day Inc., San Francisco.

Mysen B.O., Boettcher A.L. 1975. Melting of hydrous mantle: I. Phase relations of natural peridotite at high pressures and temperatures with controlled activities of water, carbon dioxide, and hydrogen. *J Petrol,* ***16***, 520-548.

Neal C.R., Taylor L.A. 1989. A negative Ce anomaly in a peridotite xenolith: evidence for crustal recycling into the mantle or mantle metasomatism. *Geochim. Cosmochint. Acta,* ***53***, 1035-1040

Niida K., Green D.H. 1999. Stability and chemical composition of pargasitic amphibole in MORB pyrolite under upper mantle conditions. *Contrib Miner Petrol* ***135,*** 18-40

Ozawa K. 1988. Ultramafic tectonite of the Miyamori ophiolite complex in the Kitakami mountains, northest Japan: hydrous upper mantle in an island arc. *Contrib Miner Petrol* ***99,*** 159-175

Peng Y. Mookherjee M. Unpublished (2020). Thermoelasticity of tremolite amphibole: geophysical implications. MSA.

Perdew J.P., Wang Y. 1986. Accurate and simple density functional for the electronic exchange energy: generalized gradient approximation. *Physical Review B,* ***33*****,** 8800-8802

Perdew J.P., Chevary J.A., Vosko S.H., Jackson K.A., Pederson M.R. Singh D.J., Fiolhais C. 1992. Atoms, molecules, solids, and surfaces: applications of the generalized gradient approximation for exchange and correlation. Physical Review B, 46, 6671-6687.

Phaneuf M.W. 1999. Application of focused ion beam microscopy to material science specimens. *Micron,****30****, 277-288*

Piermarini GJ, Block S, Barnett JD. 1973. Hydrostatic limits in liquids and solids to 100 kbar. *J Appl Phys* 6:1295-1307

Pirard C., Hermann J. 2015. Experimentally determined stability of alkali amphibole in metasomatized dunite at sub-arc pressures. *Contrib Miner Petrol* ***169,*** 1

Pollack H.N. 1986. Cratonization and thermal evaluation of the mantle. *Earth Planet, Sci. Lett.* ***80,*** 175-182

Rader, E., Emry, E., Schmerr, N., Frost, D., Cheng, C., Menard, J., Yu, C.-Q., and Geist, D. (2015), Characterization and Petrological Constraints of the Midlithospheric Discontinuity, *Geochem. Geophys. Geosyst.*, ***16***, 3484– 3504, doi:10.1002/2015GC005943.

Ran Q., Ren D., Wang Y., Tong M., Sun Y., Yan L., Dong J., Wang Z., Xu M., Li N., Peng H., Chen F., Yuan D., Xu Q., Wang S., Wang Q. 2018. Development of volcanic gas reservoirs. ISBN: 978-0-12-816132-6

Ranganathan S.I., Ostoja-Starzewski M. 2008. Universal elastic anisotropy index. *Physical Review Lett,****101***, 055504

Reed S.J.B. 2005. Electron Microprobe Analysis and Scanning Electron Microscopy in Geology (2nd Ed.). Cambridge University Press, pp. 128-162

Robinson P., Spear F.S., Schumacher J.C. 1982. Phase relations of metamorphic amphiboles: natural occurrence and theory. *Reviews in Mineralogy,* ***9B***, 4-7

Roden A.F., Murthy V.M. 1985. Mantle metasomatism. *Ann. Rev. Earth Planet. Sci,* ***13***, 269-296

Rychert C.A., Shearer P.M. 2009. A global view of the lithosphere-asthenosphere boundary. *Science,* ***324*** (5926), 495-498

Saha, S., Dasgupta, R., & Tsuno, K. (2018). High pressure phase relations of a depleted peridotite fluxed by CO_2-H_2O-bearing siliceous melts and the origin of Mid-Lithospheric Discontinuity. *Geochemistry, Geophysics, Geosystems*, 19, 595– 620.

Saha, S., Peng, Y., Dasgupta, R., Mookherjee, M., & Fischer, K. (2021). Assessing the presence of volatile-bearing mineral phases in the cratonic mantle as a possible cause of mid-lithospheric discontinuities. *Earth and Planetary Science Letters,* ***553***, 116602.

Sang L., Bass J.D. 2014. Single-crystal elasticity of diopside to 14 GPa by brillouin scattering. *Physics of the Earth and Planetary Interiors,* ***228,*** 75-79.

Schmidt M.W., Poli S. 1998. Experimentally based water budgets for dehydrating slabs and consequences for arc magma generation. *Earth Planet Sci Lett,* ***163*****,** 361-379

Selwat K., Ford H., Kelemen P. 2015. The seismic mid-lithosphere discontinuity. *Earth Planet Sci. Lett,* ***414***, 45-57

Smart K. A., Tappe S., Woodland A. B., Harris C., Corcoran L., Simonetti A. (2021). Metasomatized eclogite xenoliths from the central Kaapvaal craton a probes of a seismic mid-lithospheric discontinuity. *Chemical Geology*, ***578***, 120286

Stoops G., Marcelino V., Mees F. 2018. Interpretation of micromorphological features of soils and regoliths (2nd Ed.), Elsevier.

Sueno S., Cameron M., Papike J.J, Prewitt C.T. 1973. The high temperature crystal chemistry of trmolite. *American Mineralogist,* ***58***, 649-664

Tharimena S., Rychert C.A., Harmon N. 2016 Seismic imaging of a mid-lithospheric discontinuity beneath Ontong Java Plateau. *Earth and Planetary Science Letters,* ***450***, 62-70

Till C.B., Grove T.L., Withers A.C. 2012. The beginnings of hydrous mantle wedge melting. *Contrib. Mineral. Petrol,* ***163,*** 669-688.

Tumiati S., Fumagalli P., Tinaboschi C. Poli S. 2013. An experimental study on COH-bearing peridotite up to 3.2 GPa, and implications for crust-mantle recycling. *J Petrol,* ***54***, 453-479

Tybol H. 2006. The heterogeneous upper mantle low velocity zone. *Tectonophysics,* ***416***, 53-79.

Wallace M.E., Green D.H. 1991. The effect of bulk rock composition on the stability of amphibole in the upper mantle. *Mineral Petrol,* ***44***, 1-19

Walter D.M., Ritsema J., Yong K.W. 2012. Crustal seismicity and the earthquake catalog maximum moment magnitude (M_{cmax}) in the stable continent regions (SCRs): correlation with the seismic velocity of the lithosphere. *Earth and Planetary Science Letters,* ***357-358***, 78-83

Waters F. Erlank A. 1988. Assessment of the vertical extent and distribution of mantle metasomatism below Kimberley, South Africa. *J. Petrol*, 185-204

Weiss T., Siegesmund S., Rabbel W., Bohlen T., Pohl M. 1999. Seismic velocities and anisotropy of the lower continental crust: a review. *Pure Appl. Geophys,* ***156***, 97-122

Welch M.D., Pawley A.R. 1991. Tremolite: new enthalpy and entropy data from a phase equilibrium study of the reaction tremolite+ 2diopdie + 1.5 orthoenstatite + b-quartz + H_2O. *Amer. Min,* ***76*****,** 1931-9

Xu, W. et al. "The effect of bulk composition and temperature on mantle seismic structure." *Earth and Planetary Science Letters* 275 (2008): 70-79.

Yang H., Prewitt C.T. 2000. Chain and layer silicates at high temperature and pressures. *Reviews in Mineralogy & Geochemistry,* ***41***, 245-247

Yong T., Bina C.R., Finkelstein G.J., Zhang D., Dera P. 2019. A new high-pressure phase transition in natural gedrite. *Crystals,* ***9***, 521

Yuan H., Romanowicz B. 2010. Lithospheric layering in the North American craton. *Nature,* ***466***, 1063-1067

Zhang, J. S., & Bass, J. D. (2016). Single-crystal elasticity of natural Fe-bearing orthoenstatite across a high-pressure phase transition. *Geophysical Research Letters*, **43**, 8473– 8481.

Zhang, J. S., Bass, J. D., & Schmandt, B. (2018). The elastic anisotropy change near the 410-km discontinuity: Predictions from single-crystal elasticity measurements of olivine and wadsleyite. *Journal of Geophysical Research: Solid Earth*, **123**, 2674– 2684.